Ore Geology Reviews 92 (2018) 113–128

Contents lists available at ScienceDirect

Ore Geology Reviews

journal homepage: www.elsevier.com/locate/oregeorev

The genesis of the Liancheng Cu–Mo deposit in the Lanping Basin of SW China: Constraints from geology, fluid inclusions, and Cu–S–H–O isotopes

Changming Wang[a,b,*], Leon Bagas[b,c], Jingyuan Chen[a], Lifei Yang[a], Duan Zhang[a], Bin Du[a], Kangxing Shi[a]

[a] State Key Laboratory of Geological Processes and Mineral Resources, China University of Geosciences, Beijing 100083, China
[b] Centre for Exploration Targeting and Australian Research Council Centre of Excellence for Core to Crust Fluid Systems (CCFS), University of Western Australia, Perth, Western Australia 6009, Australia
[c] Institute of Mineral Resources, Chinese Academy of Geological Science, Beijing 100037, China

ARTICLE INFO

Keywords:
Liancheng deposit
Fluid source and evolution
Metamorphic fluids
Orogenic-type Cu–Mo deposit
Cu–S–H–O isotopes

ABSTRACT

Liancheng is an important Cu–Mo deposit hosted by red-beds in the Mesozoic to Cenozoic Lanping Basin located in the Sanjiang Tethyan Orogen of SW China. The deposit is fault controlled where it has been affected and enriched by four hydrothermal events indicated by four distinct sets of veins and their cross-cutting relationships.

A detailed Cu–S–H–O isotopic study is reported here on the mineralization focusing on the source of the metals and fluid, and on the mineralizing processes. The first two hydrothermal events are characterised by CO_2 and fluid-rich inclusions with homogenisation temperatures of 124–446 °C and salinities ranging from 0.4 to 24.6 wt% NaCl equiv. The next two hydrothermal events are characterised by liquid–rich fluid inclusions that homogenise at 145–256 °C, with salinities ranging from 1.4 to 22.9 wt% NaCl equiv. The H–O isotope values obtain from the fluid inclusions indicate that the first three hydrothermal events relate to mineralizing fluids derived from a metamorphic source, but the last event includes a mixed metamorphic and meteoric source. Chalcopyrite, tennantite, and bornite from the deposit have $\delta^{34}S$ values between −11.5 and 3‰. The $\delta^{65}Cu$ values for quartz-Cu sulfide mineralization associated with the second hydrothermal event range from −0.31 to 0.2‰, but carbonate-Cu sulfide mineralization associated with the third hydrothermal event ranges from −1.01 to −1.08‰. The combination of the Cu and S isotopic values and field observations indicate that the controlling factors include structures, the temperature of regional metamorphism, and the pH of the mineralizing fluid. The zation is, therefore, characteristic of an orogenic-type deposit.

1. Introduction

Sediment-hosted Cu-sulfide deposits are an important type of base-metal mineralization, which include disseminated, and vein-type Cu, and Cu–Fe sulfides in siliciclastic and dolomitic sedimentary rocks (e.g. Hitzman et al., 2005; Leach et al., 2005; Wang et al., 2014a). Most of this type of mineralization are regarded as the products of evolving basin-scale and fluid-flow systems, and are usually remobilised and reworked during regional deformation and metamorphism (e.g. Brown, 1978, 1997; Hitzman et al., 2005). When structurally controlled vein-type Cu deposits are hosted by siliciclastic and dolomitic rocks, they are commonly misinterpreted as sediment-hosted Cu deposits. Furthermore, structurally controlled vein-type Cu deposits are hosted by siliciclastic and dolomitic rocks that usually have different or mixed sources of mineralized fluid, such as basinal brines, and magmatic to hydrothermal or metamorphic ore-forming fluids (e.g. Vaughan et al., 1989; Beaudoin and Sangster, 1992; Polliand and Moritz, 1999; Torrealday et al., 2000; Bendezú et al., 2003; Germann et al., 2003; Baumgartner et al., 2008; Huang et al., 2016). The structurally controlled vein-type Cu deposits, thus, appear to have a more complex genesis, and are worth researching in detailed.

To better understand the genetic processes involved in the formation of structurally controlled vein-type Cu deposits in the siliciclastic and dolomitic rocks, we choose the Liancheng deposit in the eastern Himalayan-Tibetan Orogen. The mineralization is in the central part of the Mesozoic Lanping Basin and eastern part of the Indian-Asian collisional zone (Figs. 1 and 2). The deposit contains over 20 mineralized zones within the Liancheng and Jinman tectonic blocks and is hosted by parallel to subparallel fracture zones and tensile cracks within the upper member of the Huakaizuo Formation (Fig. 3; Wang, 2010).

* Corresponding author at: China University of Geosciences, No.29, Xueyuan Road, Haidian District, Beijing 100083, China.
E-mail address: wangcm@cugb.edu.cn (C. Wang).

https://doi.org/10.1016/j.oregeorev.2017.11.012
Received 3 October 2017; Received in revised form 7 November 2017; Accepted 13 November 2017
Available online 14 November 2017
0169-1368/

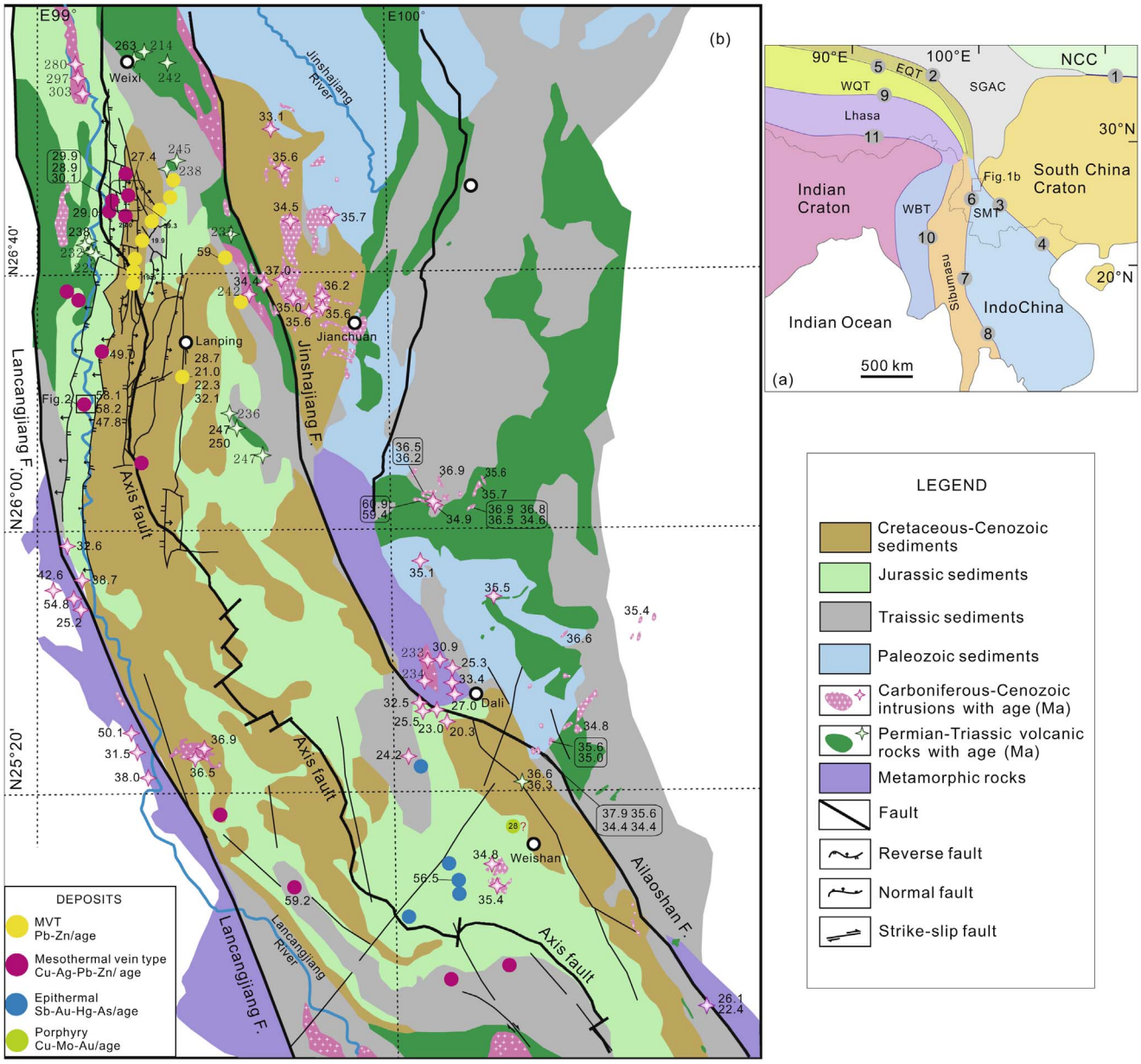

Fig. 1. Geological map of: (a) the Sanjiang-Tethys Orogen; and (b) the Lanping Basin showing the location of major ore deposits (modified after Deng et al., 2014a; Wang et al., 2014a, 2016a,b,c, 2017b). Acronyms: EQT = East Qiangtang Terrane; NCC = North China Craton; SMT = Simao Terrane; SGAC = Songpan-Ganzi Terrance; WBT = West Burma Terrane; WQT = West Qiangtang Terrane. Sutures: 1 = Qinling-Qilian-Dabie; 2 = Jinshajiang; 3 = Ailaoshan; 4 = Song-Ma; 5 = Longmu Tso-Shuanghu; 6 = Changning-Menglian; 7 = Chiang Mai-Inthanon; 8 = Bentong-Raub; 9 = Bangonghu-Nujiang; 10 = Shan Boundary; 11 = Indus-Yalung-Zangbu.

Previous studies of the Liancheng Cu–Mo deposit focused on its geology, mineralization, fluid inclusions, isotopes, and geochronology (e.g. Li and Fu, 2000; Liu et al., 2002, 2003; Bi and Mo, 2004; Xu et al., 2004; Gao et al., 2006; Chi and Xue, 2011; Zhang et al., 2013; Song et al., 2016). Despite the extent of the studies, the genesis of the deposit has not been unequivocally determined and has been classified as a syngenetic, epigenetic, or sediment-hosted stratiform Cu deposit (e.g. Li et al., 1993, 1997; Xiao et al., 1994; Yan and Li 1997; Liu et al. 2000, 2002; Wu et al. 2003; Chi and Xue, 2011; Song et al., 2016). It has also been classified as being magmatic and hydrothermal based on the interpretation that the mineralizing fluids are derived from the mantle, or a deep-seated CO_2-rich source mixed with basinal fluids (Yan and Li, 1997; Ji and Li, 1998; Que et al., 1998; Chi and Xue, 2011; Song et al., 2016). However, Hou et al. (2008) suggest that the deposit can be classified as an orogenic-type based on the interpretation that the mineralization is related to metamorphic ore-forming fluids. This disparity in the interpretation of the deposit's genesis shows that a more integrated study is necessary to understand it, which includes a better understanding of its structural, lithological, and geochemical controls.

This paper reports the geological, fluid and isotopic characteristics of the Liancheng deposit, based on new data collected during this study. The origin of the deposit is discussed with reference to ore-forming fluids, sources of metals, and structural controls on the mineralization. Finally, a comparison is made between the Liancheng and sediment-hosted Cu deposits elsewhere on Earth. This contribution concludes with an interpretation of the deposit's genesis, and it significant for mineral exploration aiming to discover large-scale deposits hosted by red-bed sedimentary basins in the eastern Himalayan-Tibetan Orogen.

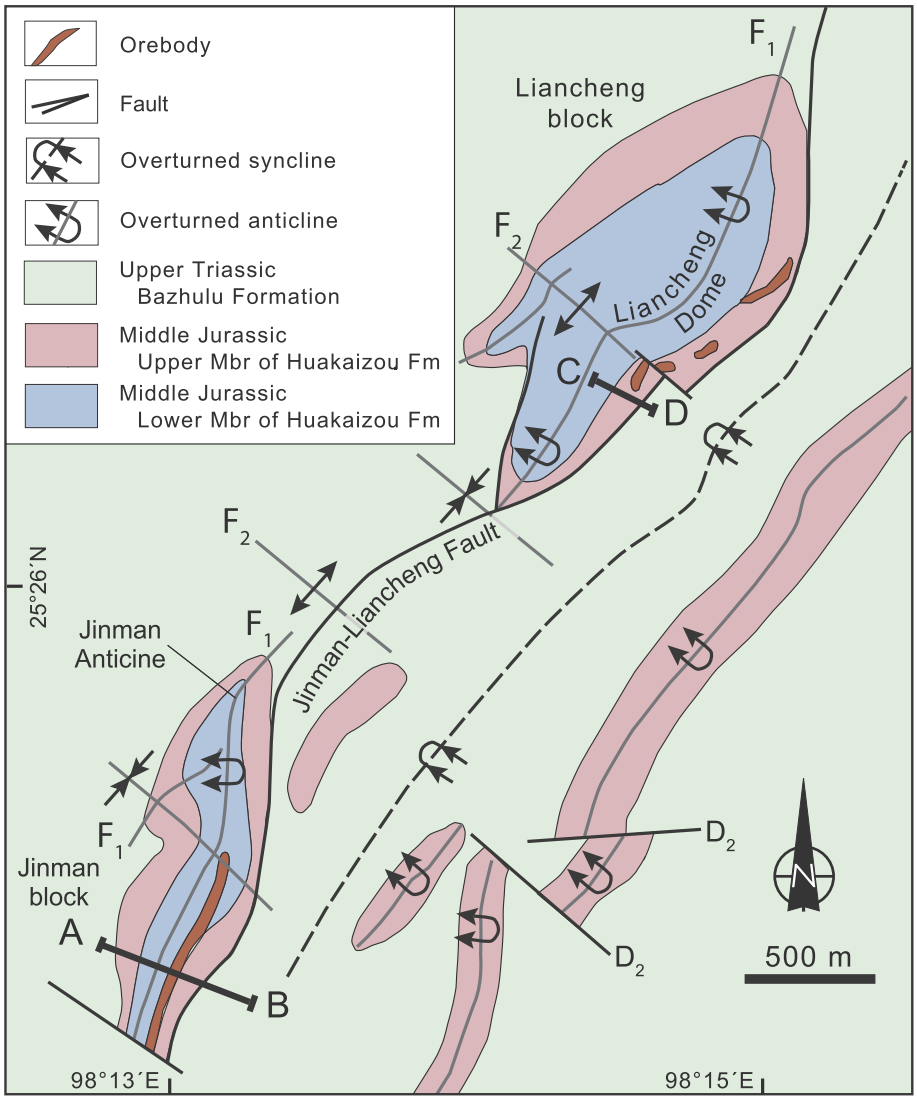

Fig. 2. Geological map of the Liancheng Cu–Mo deposit (modified after Li and Fu, 2000). Section A–B and C–D are included in Fig. 3.

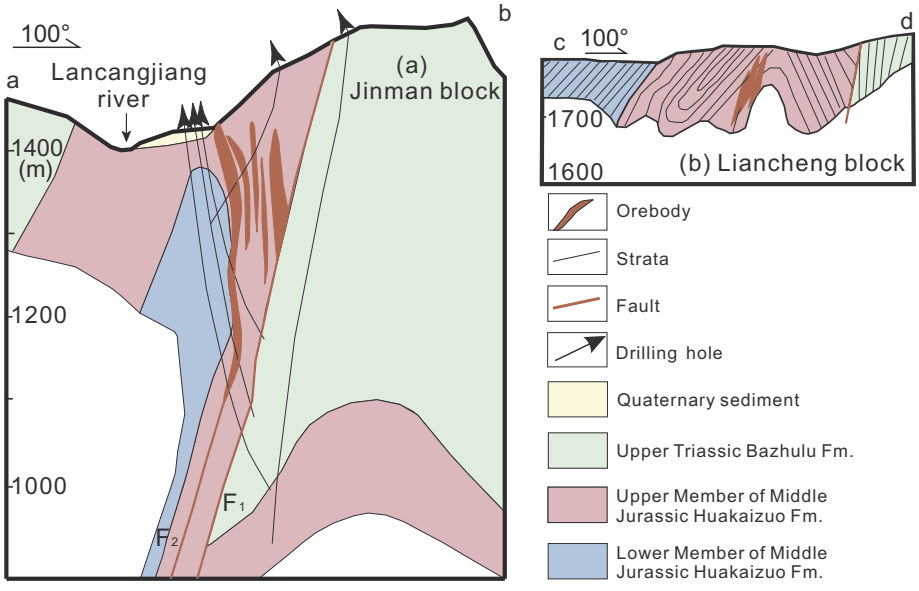

Fig. 3. Geology of: (a) section A–B in the Jinman block, and (b) section C–D in the Liancheng block (modified from Li and Fu, 2000; Gao et al., 2006).

2. Regional geological setting

2.1. Location and regional geological evolution

Major terranes in the Sanjiang Tethyan Orogen and adjacent areas include the Tengchong-Baoshan, Simao, and Yangtze terranes, which are separated by sutures such as the Jinshajiang-Ailaoshan and Changning-Menglian sutures (Du et al., 2016; Deng et al., 2016, 2017). The Mesozoic to Cenozoic Lanping Basin in the northern part of the Simao Terrane is bound by the Changning-Menglian Suture to the west, and Jinshajiang-Ailaoshan Suture to the east (Fig. 1; Wang et al., 2014a,b).

The tectonic history of the Lanping Basin is complex and includes rifting of the Simao Terrane from the Cathaysian continent during the early Ordovician to Middle Devonian, formation of a foreland-basin during the Middle Permian to Middle Triassic, followed by post-collision extension and development of a rift basin during the Late Triassic (ca. 235–203 Ma). This was followed by the development of a sag basin during the Jurassic to Cretaceous, a foreland basin during the Paleocene to Early Oligocene, and collisional tectonics during the collision of the Indian and Asian continents at ca. 55–50 Ma (Dupont-Nivet et al., 2010; Najman et al., 2010; Deng et al., 2014a,b; Wang et al., 2015b, 2016a).

2.2. Stratigraphy

The region around the Lanping Basin includes Precambrian gneissic granulite, schist, and marble. These high-grade rocks are unconformably overlain by low-grade Early Ordovician slate, phyllite, quartzite and marble which, in turn, are unconformable overlain by Middle Devonian to Triassic conglomerate, shallow marine and continental sedimentary rocks. The youngest rocks are Mesozoic red-beds in the Lanping Basin (Third Geological Team, 1984).

2.3. Major structures

The most prominent structures affecting the Lanping Basin are thrust-nappes related to the Early Cenozoic collision of the Indian and Asia continents (e.g. Zhu et al., 2005). The thrust-nappes are directed approximately E-W and dip to the east or west in Paleogene-Neogene basins (Spurlin et al., 2005). In addition, subsequent Eocene-Miocene transpression resulted in the formation of Cenozoic strike-slip faults, such as the Ailaoshan Fault along the eastern margin of the Lanping Basin, and a series of its secondary faults within the basin (Fig. 1).

2.4. Magmatism

Permian to Triassic magmatic events are recognized along the eastern and western margins of the Lanping Basin, but no magmatism is found in the Liancheng-Jinman area (Fig. 1). The Permian to Triassic magmatism is represented by basalt, andesite and rhyolite in the Late Permian to Early Triassic Pantiange and Triassic Manghuai formations with zircon U–Pb zircon dates ranging from ca. 258 to 229 Ma. Volcanism continued in the Simao Basin with extrusion of basalt in the ca. 210 Ma Manghuihe Formation (Wang et al., 2010; Fan et al., 2014; Yang et al., 2014; Liang et al., 2015). Permian–Triassic magmatic rocks are widespread along both margins of the basin including the ca. 230–214 Ma Ludian and ca. 261–203 Ma Lincang batholiths (Wang et al., 2015a; Deng et al., 2017).

The Middle Eocene to Early Oligocene was the most important period for the emplacement of potassic to ultra potassic magmatic rocks along the eastern margin of the Lanping Basin, with U–Pb zircon dates ranging from ca. 41 to 34 Ma (Fig. 1; Zeng et al., 2006; Lu et al., 2012, 2013). This includes Eocene–Oligocene potassic to ultra potassic granitic rocks associated with porphyry Cu–Mo–Au deposits with molybdenite Re–Os isochron dates between ca. 40 and 34 Ma (e.g. Zeng et al., 2012; Liang et al., 2007, 2008; Lu et al., 2013; Deng et al., 2015a,b).

3. Deposit geology

The Middle Jurassic Huakaizuo and Late Jurassic Bazhulu formations are host rocks in the Liancheng mineralized area (Fig. 2). The Huakaizuo Formation consists of purple-red conglomerate interbedded with pebbly sandstone and sandstone at the base, and sandstone interbedded with shale at the top. The Bazhulu Formation consists of purple-red shale interbedded with sandstone. The shale has been metamorphosed into slate at a low-grade metamorphism.

The most prominent structural feature in the mineralized Liancheng district is an NNE-striking anticline with an upright western limb and overturned eastern limb (Fig. 2). The folds are associated with NNE-trending reverse faults dipping 65–85° NW parallel to the axis of the fold (Fig. 3). In addition, there are some relatively late NW-trending strike-slip faults, which cut the NNE-trending reverse faults and folds (Fig. 2).

The Liancheng deposit is subdivided into the Liancheng and Jinman orebody clusters and several other segments (Fig. 2). The Liancheng and Jinman orebody clusters are located near the core of the Liancheng and Jinman anticlines, particularly above the NNE-trending first-generation reverse (D_1) fault on the eastern limb of the overturned fold (Fig. 3). Most orebodies are hosted by layer-parallel shears and tensile fractures within the upper member of the Huakaizuo Formation (Figs. 2 and 3).

The No. 1 orebody in Jinman block is the richest in both blocks, and is hosted by layer-parallel shears at the contact between the lower and upper members of the Huakaizuo Formation (Figs. 2 and 3). The mineralization is stratabound and in a stockwork, with grades ranging between 0.65 and 12.02% Cu, and 21.9 g/t Ag. The mineralization averages 8 m in thickness, is at least 1350 m long, and dips 70–85° NW (Wang, 2010). In addition, a series of small scale orebodies in the Jinman block are distributed within tensile cracks and cleavage in the upper member of the Huakaizuo Formation (Fig. 3b), where it is 35 m long and 0.7–17.3 m wide with a grade ranging from 0.3 to 2.68% Cu and 2.6–10.8 g/t Ag (Wang, 2010).

The Liancheng block, located to the NE of the Jinman block, hosts a series of small orebodies distributed in layer-parallel shears and tensile cracks in the upper member of the Huakaizuo Formation (Figs. 2 and 3), which form a 17.5 m thick zone averaging 0.8% Cu (Wang, 2010).

There are many sulfide and gangue minerals in both of the blocks' mineralized zones including the major assemblage chalcopyrite – tetrahedrite – bornite – tennantite, and minor assemblage of chalcocite – pyrite – sphalerite – galena. In addition, fine-grained molybdenite is present in the Liancheng block. The gangue minerals are dominantly quartz, calcite, ankerite, sericite, and minor graphite, and alteration characterised by the assemblage sericite – silica – carbonate – graphite.

Four hydrothermal events represented by quartz (-carbonate) vein sets have been identified in the area and are distinguished from each other by their cross-cutting relationships. It is not certain what the ages of these vein sets are, and it is acknowledged that they might represent a single progressive hydrothermal fluid, but they are here regarded as separate events until they can be properly dated.

The hydrothermal event is represented by early white quartz veins with minor amounts of carbonate, followed by quartz – chalcopyrite – molybdenite (-tennantite-bornite), and carbonate – tennantite (-chalcopyrite-bornite), and finally carbonate (-minor quartz) (Figs. 4a–h, 5a–h, and 6). The quartz veins contain minor amounts of carbonate and fill layer-parallel shears and tensile fractures (Fig. 4a, b). These veins are cut by veins of Cu-minerals that also fill vugs and open-space cavities, and are included in the second hydrothermal event (Fig. 4c). This early veining has been interpreted as being "syn-mineralization" (Song et al., 2016), but we now know that this is not the case.

The second hydrothermal event is the main Cu–Mo mineralizing event represented by large amounts of chalcopyrite, tetrahedrite, bornite, and molybdenite hosted by euhedral quartz. The mineralization is commonly concentrated as selvedges along the contact between the

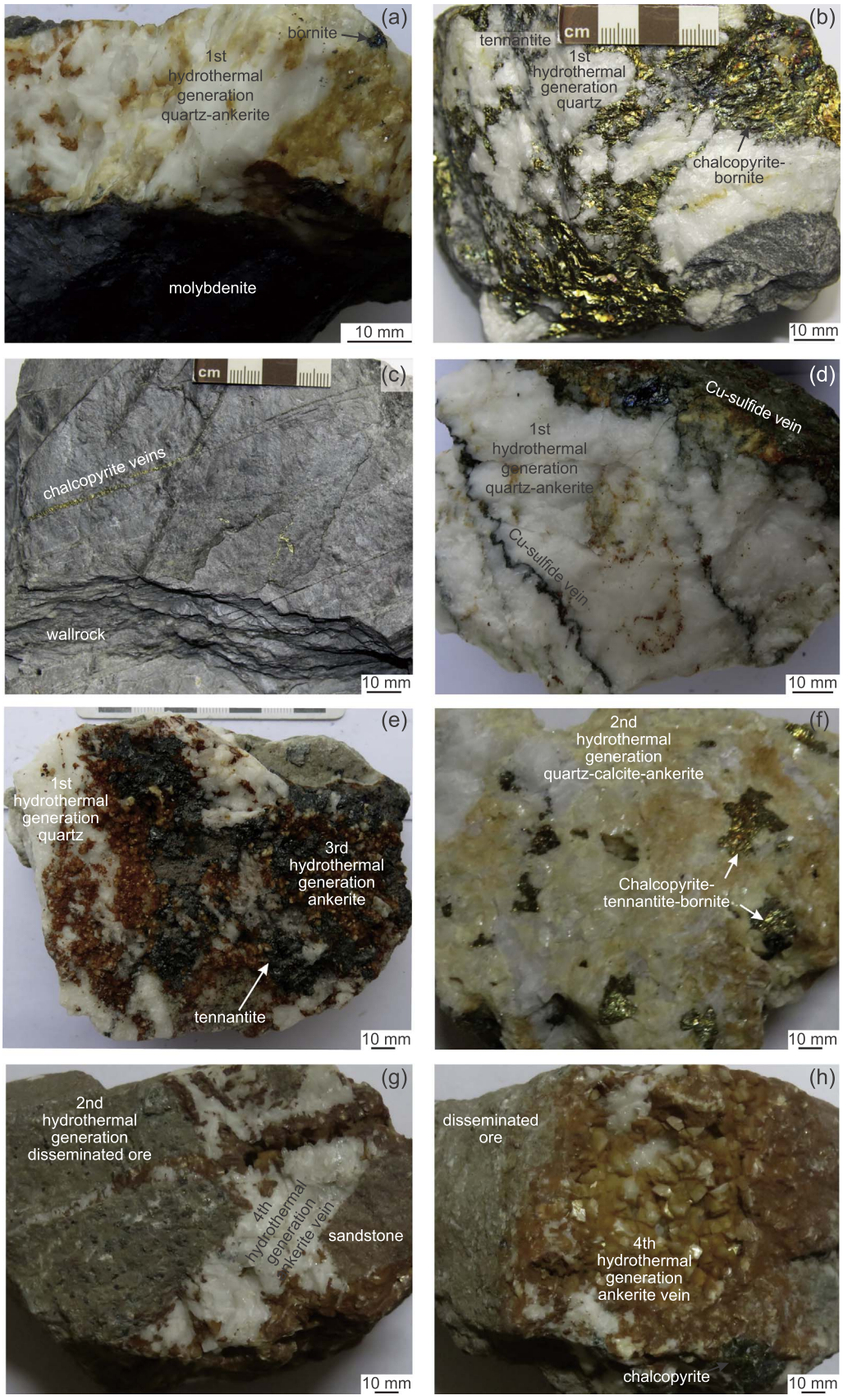

Fig. 4. Macroscopic features of samples collected from mineralization at the Liancheng Cu–Mo deposit: (a) Mo and Cu minerals in quartz filling fractures; (b) Cu minerals in brecciated the first generation of hydrothermal quartz; (c) Cu-sulfide vein in slate; (d) second generation Cu-sulfide vein in a fractured first generation quartz veins; (e) tennantite-ankerite from the third hydrothermal event cementing brecciated first generation quartz; (f) chalcopyrite-tennantite-bornite-ankerite from the second hydrothermal event; (g) Quartz-ankerite vein from the fourth hydrothermal event cutting mineralization from the second event; and (h) quartz-ankerite from the fourth hydrothermal event.

quartz and country rocks, and sulfidic quartz veins crossing and metasomatising the early quartz veining (Figs. 4b, c and 5a–f).

The third hydrothermal pulse is also characterised by sulfide mineralization represented by the assemblage carbonate – tetrahedrite – chalcopyrite – bornite – pyrite (Figs. 4e and 5g, h). Euhedral pyrite coexists with carbonate in places, with chalcopyrite forming fracture fills in pyrite (Fig. 5g). The chalcopyrite commonly cuts the second-generation quartz-Cu sulfide veins (Fig. 5 h).

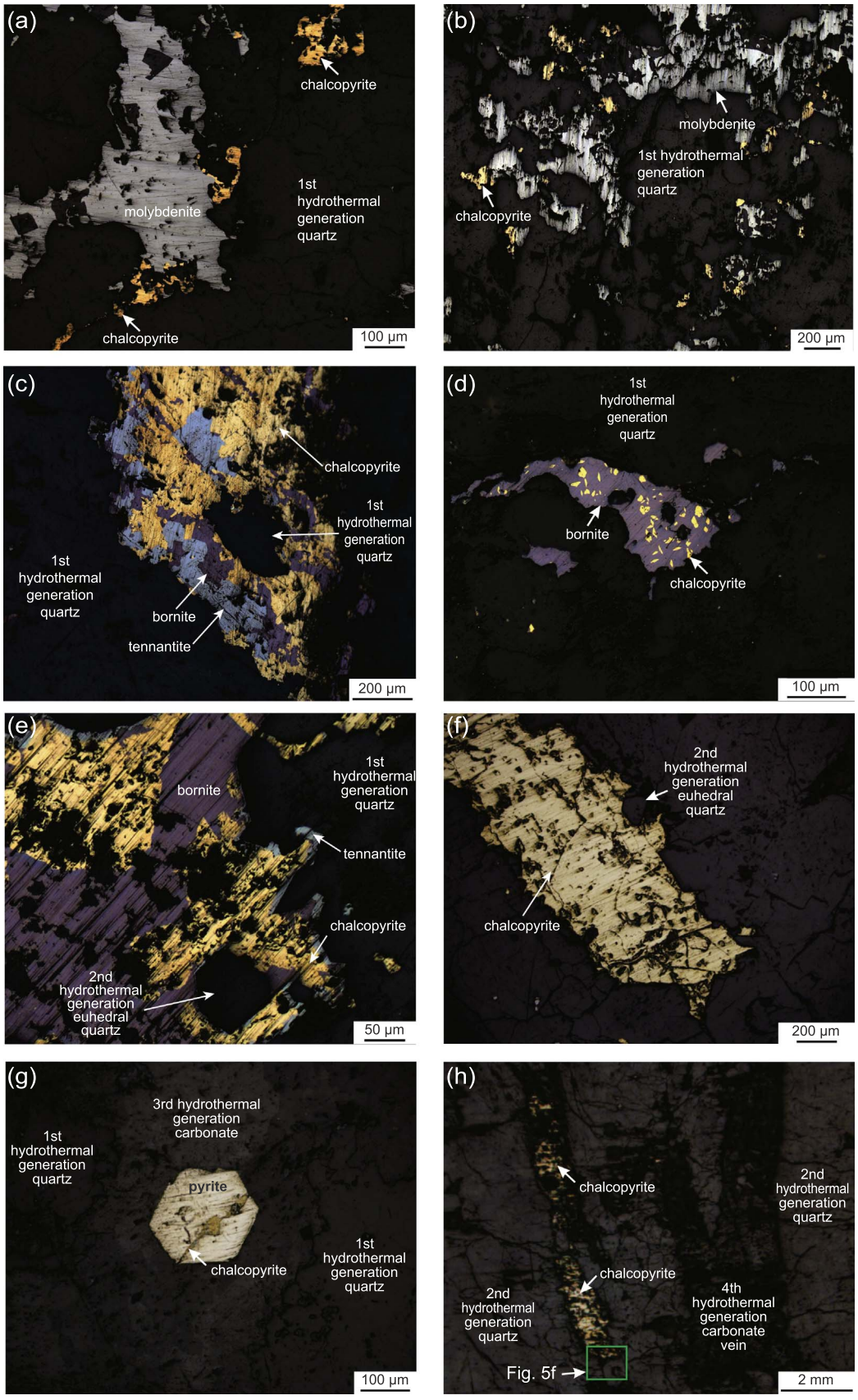

Fig. 5. Photomicrographs of the mineralization at the Liancheng Cu–Mo deposit: (a) and (b) chalcopyrite and molybdenite in quartz-filled fractures replacing quartz related to the first hydrothermal event; (c) chalcopyrite-tennantite-bornite replacing first generation quartz; (d) bornite hosted by fractures in first generation quartz; (e) second hydrothermal chalcopyrite-bornite-quartz; (f) chalcopyrite co-existing with second generation euhedral quartz; (g) third hydrothermal euhedral pyrite co-existing with carbonate minerals, and chalcopyrite veining pyrite; and (h) carbonate vein representing the third hydrothermal event cutting second generation quartz-sulfide.

The last hydrothermal event is not mineralized and represented by ankerite veining crossing the earlier three vein sets. The ankerite veins also fill vugs and open-space cavities forming euhedral and granular textures growing inward in the vugs and openings (Fig. 4 g, h). This vein set is interpreted to have formed at shallow depths. The minerals associations for each hydrothermal event are shown in Fig. 6.

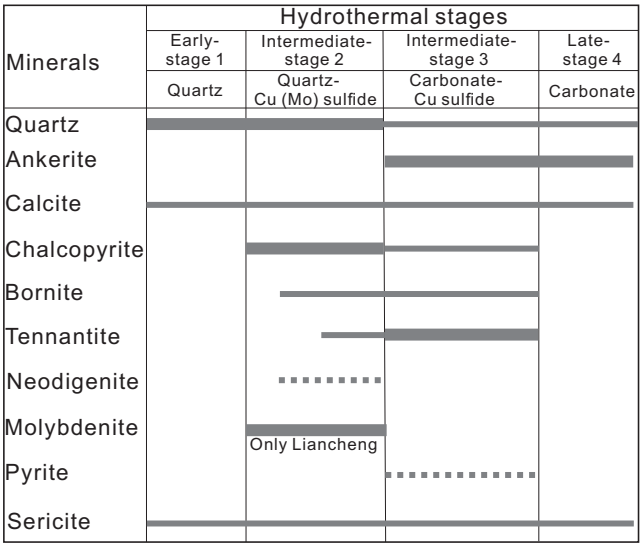

Fig. 6. Mineral paragenesis at the Liancheng Cu–Mo deposit.

4. Analytical methods

Samples were collected from the mine in the Liancheng block at the 1200 and 1300 m levels, and outcrops in the block at an elevation of ~1800 m. The samples were crush and sulfides were separated using a combination of heavy liquid, magnetic and hand-picking techniques. The extracted sulfides were then checked using X-ray diffractometry to ensure their purity.

4.1. Fluid inclusion

Thirty samples of quartz and carbonate were collected from the different generations of veining for fluid inclusion studies. The characteristics of the inclusions polished thin sections were microscopically accessed for their relative age, shape, size, and style of distribution. The fluid inclusions were then microthermometrically measured using a Linkam MDS 600 heating-freezing stage equipped with a Zeiss microscope, and Laser Raman spectroscopic analyses were carried out at the Deposit Geology Institute, Chinese Academy of Geological Sciences in Beijing (CAGS). The measurements consist of the first ice melting temperature (T_m), melting of carbonic hydrite ($T_{m,\ cla}$), ice-melting temperature ($T_{m,\ ice}$), and homogenisation temperature (T_h). Salinities of aqueous two-phase inclusions were calculated from the measured final ice-melting temperatures using the reference data of Bodnar (1993) for the NaCl-H_2O system, and salinities of hypersaline inclusions were calculated from measured halite-melting temperatures using the equation of Lecumberri-Sanchez et al., 2012.

4.2. H–O isotopes

Analyses of the hydrogen and oxygen isotopic compositions were carried out using a MAT-251 mass spectrometer with analytical precisions of ± 0.2‰ for the O-isotopes and ± 2‰ for the H-isotopes at the Deposit Geology Institute, CAGS. The δD values were analysed using the decrepitating method on primary fluid inclusions in quartz. The $\delta^{18}O_{H2O}$ values were calculated using the formula $1000\ln\alpha_{quartz\text{-}water} = 3.38 \times 10^6/T^2 - 3.40$ and the corresponding homogenisation temperatures of the primary fluid inclusions (Clayton et al., 1972)

4.3. Cu isotopes

All samples collected for Cu-isotope analyses were from the Jinman block (Table 2). Around ~20 mg of samples containing at least 0.4 μg Cu were dissolved with 1 ml of 8 N HCl and +0.001% H_2O_2 at a temperature of ~160 °C in screw-top Teflon containers. The Cu mineral was purified using single column ion exchange chromatography with the Bio-Rad strong anion resin AG-MP-1M (Maréchal et al., 1999). The Cu isotope analyses were completed using the *Neptune plus* MC-ICP-MS at the Isotope Geochemistry Laboratory of the China University of Geosciences Beijing (CUGB) following the procedure described by Liu et al. (2014). The Cu isotope ratios in this study are reported as $\delta^{65}Cu$ values relative to the NIST976 Cu standard ($^{65}Cu/^{63}Cu = 0.4456 \pm 0.0004$) using the equation $\delta^{65}Cu = (((^{65}Cu/^{63}Cu)_{sample}/(^{65}Cu/^{63}Cu)_{standard} - 1) \times 1000$ (Liu et al., 2014). The accuracy of the $\delta^{65}Cu$ analyses are estimated to be better than 0.05‰ (2σ).

4.4. S isotopes

Sulfur isotopic analyses of sphalerite, galena and pyrite separates from the study area were carried out at the Laboratory for Stable Isotope Geochemistry, Institute of Geology and Geophysics, Chinese Academy of Sciences (CAS). The analyses were carried out using 200-mesh pure separates of chalcopyrite, tetrahedrite, and bornite, which were combusted with CuO, Cu_2O and V_2O_5 in an oven at 1000 °C and under vacuum conditions. Liberated $SO_{2\ gas}$ was frozen in a liquid nitrogen trap. After cryogenic separation from other gases, the sulfur isotopic compositions were measured with the Canyon Diablo Troilite (CDT) standard on a MAT-253 mass spectrometer with an analytical precision of ± 0.2‰. The routine analytical precision for the standard material was ± 0.2‰. The results were then calibrated against the standard with a routine analytical precision of ± 0.2‰.

5. Results

5.1. Fluid inclusion data

All samples contain abundant primary and secondary inclusions, with irregular, ovoid, and negative crystal forms, and only primary inclusions were analysed in this study, as defined by Roedder (1984). Four types of primary inclusions are recognised, based on their textural, relative paragenesis, and the proportion of their phases at room temperature. These are liquid-rich inclusions with gas bubbles, three-phase CO_2-bearing inclusions, vapour-only inclusions, and liquid-only inclusions (Fig. 7).

Liquid-rich (L-type) inclusions are the most common type, and found in all of the quartz-carbonate veins generations in the study area. They consist of a liquid phase (L_{H2O}) and a smaller proportion of vapour bubble (V_{H2O}), and vary in shape from native-crystal to highly irregular (Fig. 7). This type of inclusion homogenises to liquid, and rarely to vapour, and is much smaller in size relative to the other inclusion types being 1–20 μm across, and have a vapour volume between 5 and 40%.

The CO_2-bearing (C-type) inclusions are present in quartz from the first and second hydrothermal generation (Fig. 7a, d, f, g), consist of liquid + vapour + CO_2 with negative crystal shapes, and vary between 3 and 14 μm in size. The vapour-only inclusions are present in quartz veins representing the second hydrothermal generation, are 3–8 μm across, and are three-phase CO_2-bearing inclusions.

Liquid-only inclusions are 2 to 6 μm across and are only present in the quartz-carbonate veins representing the fourth hydrothermal event. The microthermometric data and calculated parameters for fluid inclusions are summarized in Table 1 and graphically illustrated in Figs. 8 and 9.

5.1.1. First generation quartz

Fluid inclusions in the first quartz generation homogenise between 160-446 °C with a modal distribution between 200 and 300 °C, and have salinities ranging from 0.4 to 22.5 wt% NaCl equiv (concentrating at 8 to 20 wt% NaCl equiv).

All of the L-type inclusions have homogenisation temperatures ranging from 160 to 351 °C (Fig. 8), and have melting temperatures

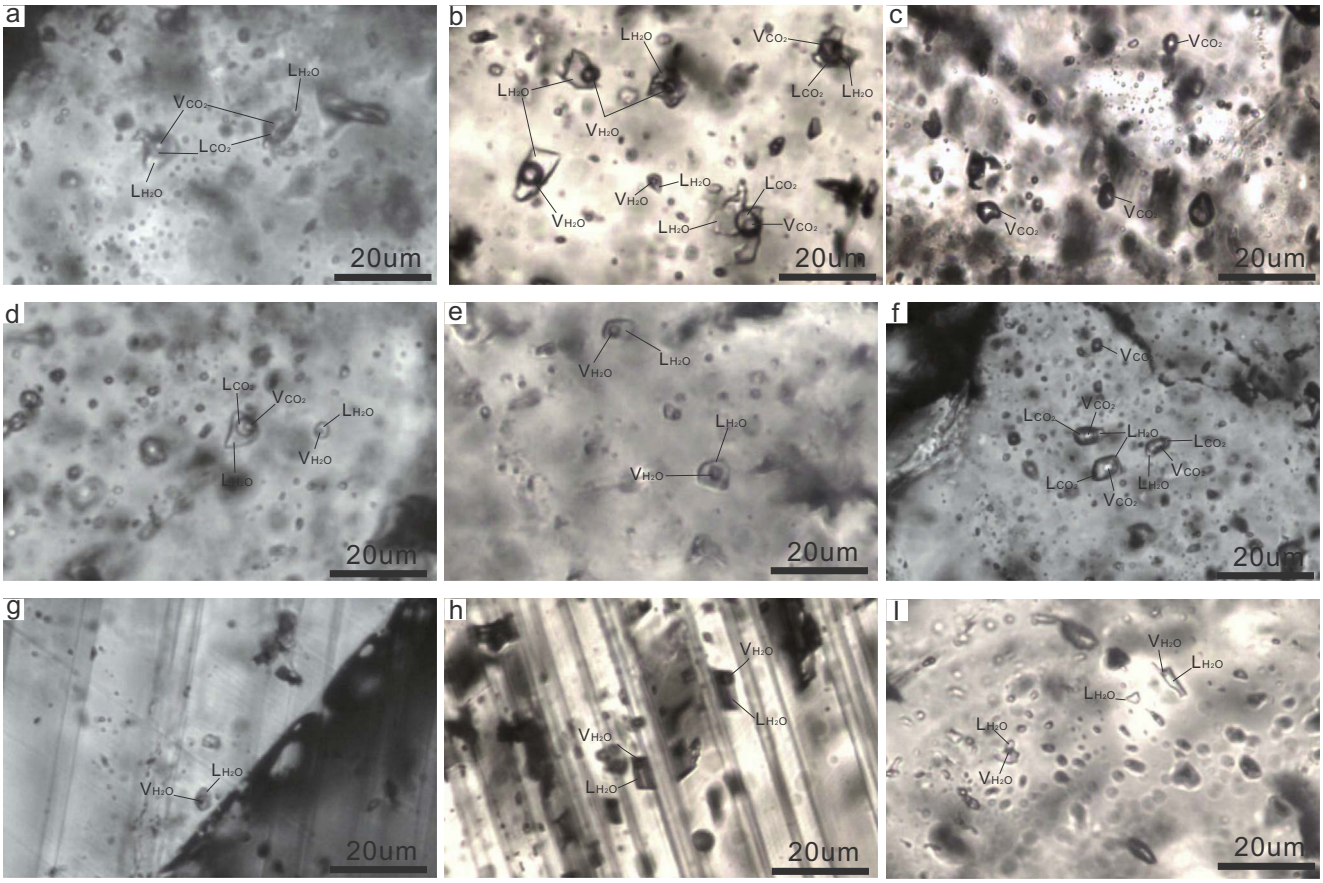

Fig. 7. Photomicrographs showing the types and distribution of fluid inclusions in mineralized quartz from the Liancheng Cu–Mo deposit: (a) CO_2-bearing three-phase inclusions from first generation quartz (sample LC15D03B1-1A); (b) CO_2-bearing three-phase inclusions coexisting with liquid-rich two-phase inclusions from the first generation quartz (sample JM15D02B1-2); (c) vapour-only inclusions from the first generation quartz (sample LC15D03B3-C); (d) CO_2-bearing three-phase inclusions coexisting with liquid-rich two-phase inclusion from quartz related to the second hydrothermal event (sample LC15D03B5-3B); (e) liquid-rich two-phase aqueous inclusions from second generation quartz (sample JM15D09B3) (f) CO_2-bearing three-phase inclusions coexisting with vapour-only inclusions from second generation quartz (sample LC15D03B5-3B); (g) liquid-rich two-phase fluid inclusions in carbonate from the third hydrothermal event (sample JM15D03B5-1); (h) liquid-rich two-phase fluid inclusions in carbonate from the fourth hydrothermal event (sample JM15D08B11); (i) liquid-rich inclusions and liquid-only inclusions in carbonate from the fourth hydrothermal event (sample JM15D08B11).

Table 1
Summary of microthermometric data and calculated parameters for fluid inclusions from the Liancheng Cu–Mo deposit.

Stage	Mineral	FIT	Size (μm)	$T_{m,\ CO2}$ (°C)	$T_{m,\ ice}$ (°C)	Th (°C)	Salinity (wt%)
1	Quartz	Two-phase	1–20	No	-0.5 to −19.8	160–351	6.3–22.5
		Three-phase	4–14	5.4 ~ 7.3	No	278–446	0.4–11.6
2	Quartz	Two-phase	2–18	No	−1.9 to −22.9	124–371	3.2–24.6
		Three-phase	5–12	3.3 ~ 9.8	No	268–407	5.2–8.4
3	Carbonate	Two-phase	2–8	No	−0.8 to −20.3	152–259	1.4–22.9
4	Carbonate	Two-phase	2–12	No	−1.4 to 10.0	145–259	2.4–14.0

Table 2
Hydrogen and oxygen isotopic compositions of quartz from Cu–Mo ore at the Liancheng deposit. The $\delta^{18}O_{H2O}$ values were calculated from those of quartz on the basis of the isotope fractionation equation of $1000\ln\alpha_{quartz\text{-}water} = 3.38 \times 10^6/T^2 - 3.40$ (Clayton et al., 1972). Abbreviations: Qz = quartz; Th = homogenisation temperature.

Sample assemblage	Mineral	Stage	δD_{H20} (SMOW ‰)	$\delta^{18}O$ (‰)	Th (°C)	$\delta^{18}O_{H20}$ (‰)
Quartz-Cu mineral	Quartz	2	−64.0	18.6	237	9.0
Quartz-Cu mineral	Quartz	2	−109.7	17.3	237	7.7
Quartz-Cu mineral	Quartz	2	−122.2	16.0	237	6.4
Quartz-Cu mineral	Quartz	2	−117.0	16.3	237	6.9
Quartz-Cu mineral	Quartz	2	−87.9	17.4	237	7.8
Carbonate-Cu mineral	Quartz	3	−76.0	16.6	222	6.2
Carbonate-Cu mineral	Quartz	3	−95.0	16.9	222	6.5

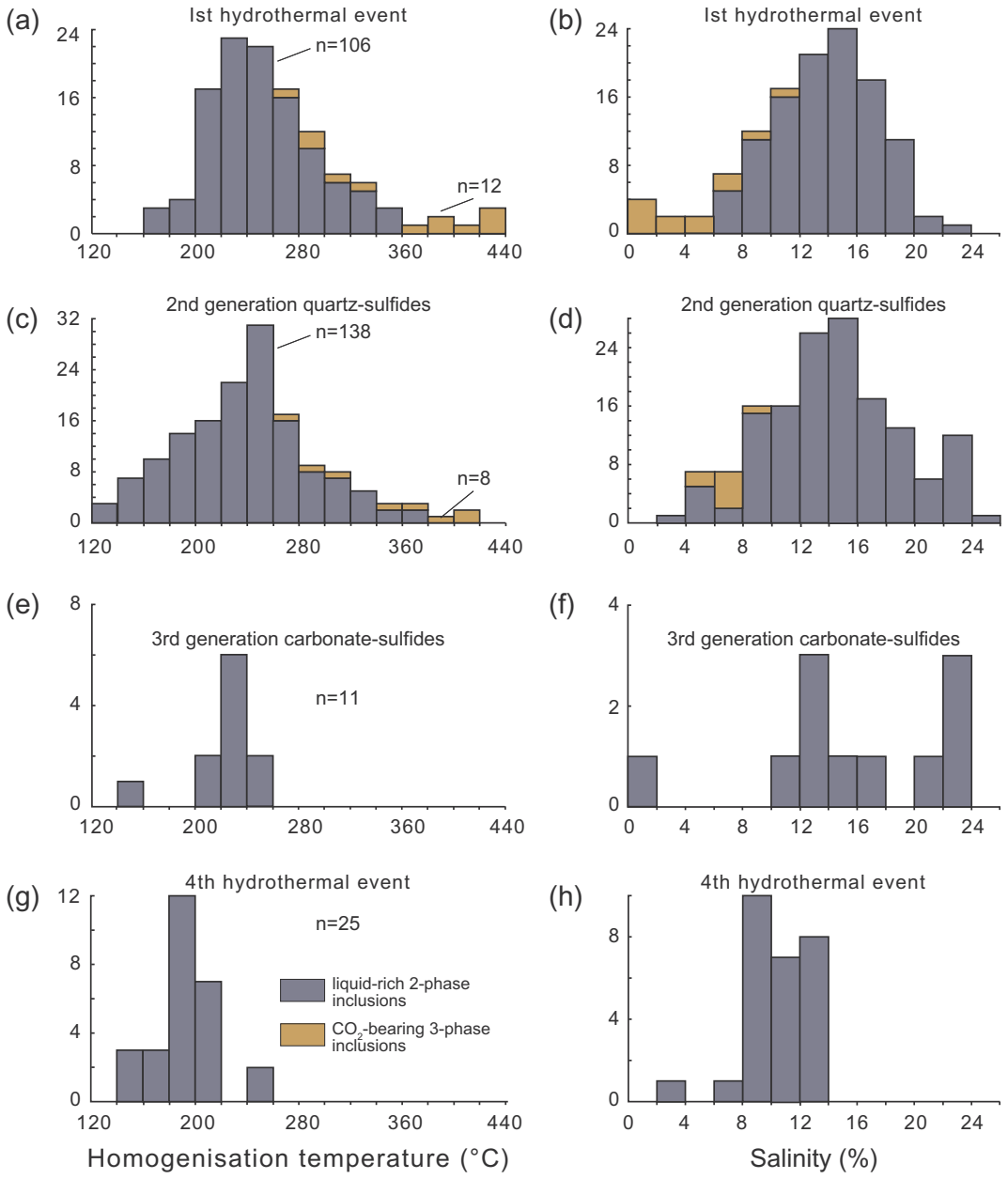

Fig. 8. Histograms of homogenisation temperatures and salinity for all of the inclusion types from the four hydrothermal events at the Liancheng Cu–Mo deposit.

between −19.8 and −0.5 °C, corresponding to salinities of 0.9–22.5 wt % NaCl equiv (Bodnar, 1993) (Table 1). For C-type inclusions and vapour-only inclusions are commonly present at the same time, indicating they are coeval and representing phase immiscibility during inclusion trapping (Fig. 7). All of the C-type inclusions homogenise to a fluid at temperatures between 278 and 446 °C (Fig. 8), and have a salinity of 0.4–11.6 wt% NaCl equiv (Collins, 1979) (Table 1; Fig. 9).

5.1.2. Second generation quartz

Fluid inclusions in the second hydrothermal generation of quartz homogenise at 124–407 °C with a modal distribution of 160–280 °C, and salinities ranging from 3.2 to 24.6 wt% NaCl equiv with a modal distribution of 8–24 wt% NaCl equiv.

The L-type inclusions homogenise at 124–371 °C (Fig. 8), and have melting temperatures between −22.9 and −1.9 °C, corresponding to salinities of 3.2–24.6 wt% NaCl equiv (Bodnar, 1993; Table 1).

All of the C-type inclusions homogenise to the temperatures from 268 to 407 °C, and have salinities between 5.2 and 8.4 wt% NaCl equiv. (Collins, 1979; Figs. 8 and 9; Table 1).

5.1.3. Carbonate from the third hydrothermal event

Carbonate representing the third hydrothermal event contains L-type inclusions that homogenise from 153 to 259 °C (Fig. 8), and have melting temperatures between −20.3 and −0.8 °C, corresponding to salinities of 1.4–22.9 wt% NaCl equiv. (Bodnar, 1993; Table 1).

5.1.4. Carbonate from the fourth hydrothermal event

L-type inclusions from the fourth-generation vein set homogenised to a fluid at temperatures ranging from 144.8 to 258.8 °C (Fig. 8), and have melting temperatures of between −10 and −1.4 °C corresponding to salinities of 2.4–13.5 wt% NaCl equiv. (Bodnar, 1993; Table 1).

5.2. Oxygen and hydrogen isotope data

The oxygen and hydrogen isotopic analyses of quartz and carbonate are listed in Table 3 and plotted in Fig. 10. The $\delta^{18}O$ quartz and

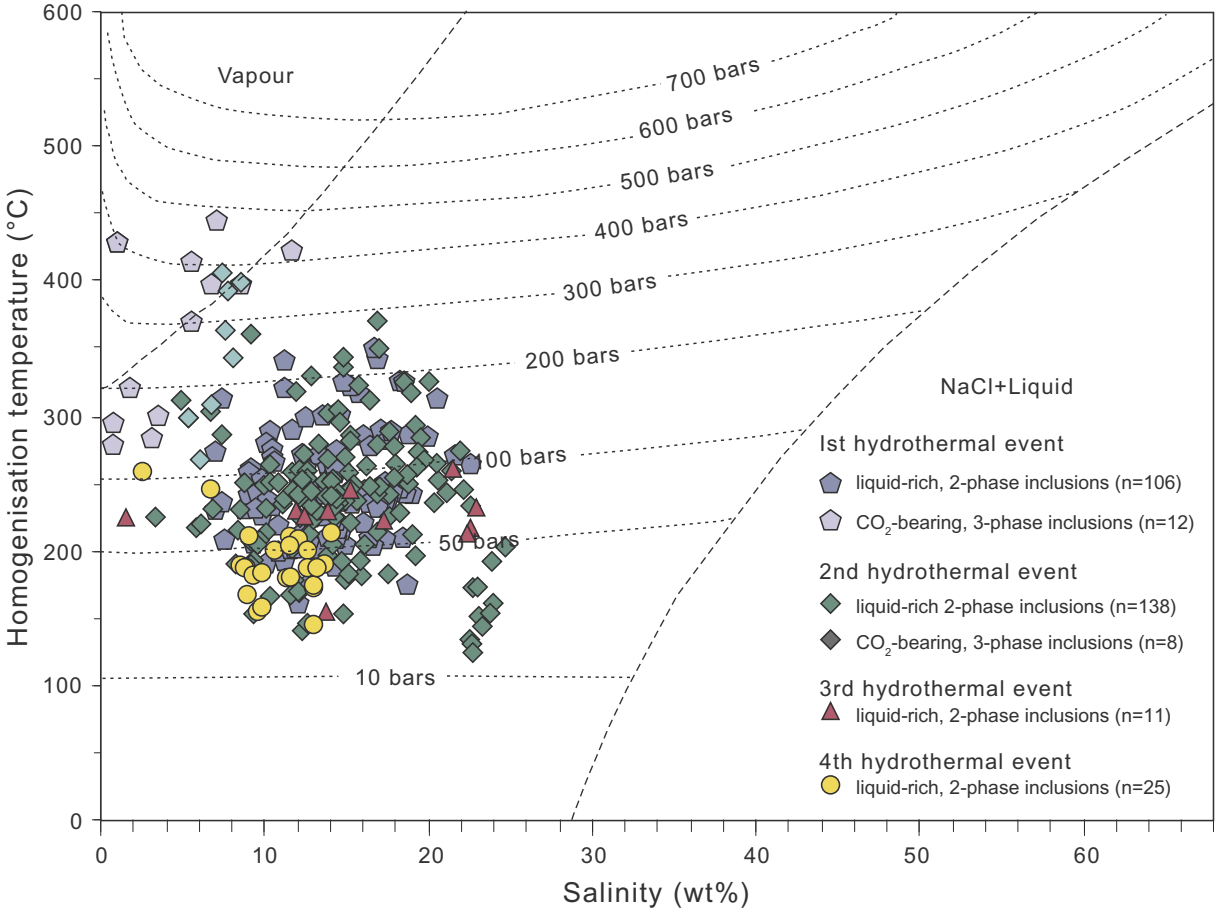

Fig. 9. Summary plot of homogenisation temperatures, salinities, and pressure of fluid inclusions related to the fourth hydrothermal events at the Liancheng Cu–Mo deposit. Isobars were calculated from the equations of Driesner and Heinrich (2007).

carbonate values range from 7.8 to 15.6‰, and the δD values from fluid extracted from inclusions in the quartz and carbonate range from −84 to −48‰ (Table 2; Fig. 10). The $\delta^{18}O$ quartz and carbonate values in the first generation of quartz-carbonate veining are 7.8–11.3‰ with δD values of −64 to −48‰, and those from Ag-bearing galena and sphalerite in the second quartz generation are 9.5–11.9‰ with δD values between −72 and −62‰.

5.3. Cu isotope data

The $\delta^{65}Cu$ values determined from 13 sulfide samples are listed in Table 3 and plotted in Fig. 11. The $\delta^{65}Cu$ values range from −1.08 to 0.2‰ with an average of −0.25‰. However, sulfide minerals in carbonate hosting Cu have $\delta^{65}Cu$ values peaking at −1.05‰, and those from mineralized quartz peak at −0.03‰. The $\delta^{65}Cu$ chalcopyrite values range from −0.09 to 0.2‰, and tetrahedrite has a variable isotopic $\delta^{65}Cu$ composition ranging from −1.08 to 0.06‰. The $\delta^{65}Cu$ isotopic value for bornite is relatively heavy averaging −0.31‰.

Table 3
Cu–S isotopic data (‰) for Cu minerals from the Liancheng Cu–Mo deposit.

Mineral assemblage	Stage	Mineral	$\delta^{34}S_{V\text{-}CDT}$‰	$\delta^{65}Cu$‰	2SD
Quartz-Cu mineral	2	Chalcopyrite	1.1	−0.04	0.03
Quartz-Cu mineral	2	Chalcopyrite	−4.8	0.02	0.01
Quartz-Cu mineral	2	Chalcopyrite	−11.5	−0.15	0.09
Quartz-Cu mineral	2	Chalcopyrite	−2.9	0.20	0.08
Quartz-Cu mineral	2	Chalcopyrite	−2.5	−0.09	0.07
Quartz-Cu mineral	2	Chalcopyrite	−3.8	0.16	0.03
Quartz-Cu mineral	2	Chalcopyrite	−11.3	0.10	0.01
Quartz-Cu mineral	2	Bornite	0.9	−0.31	0.01
Quartz-Cu mineral	2	Tetrahedrite	−3.6	−0.11	0.04
Quartz-Cu mineral	2	Tetrahedrite	−10.0	0.06	0.06
Carbonate-Cu mineral	3	Tetrahedrite	2.2	−1.08	0.04
Carbonate-Cu mineral	3	Tetrahedrite	2.1	−1.04	0.05
Carbonate-Cu mineral	3	Tetrahedrite	3.0	−1.01	0.01

5.4. Sulfur isotope data

The $\delta^{34}S$ values determined from 13 sulfide samples are listed in Table 3 and plotted in Fig. 11. The $\delta^{34}S$ values of sulfides in the mineralized zones range from −11.5 to 3‰ with an average of −3.2‰. In contrast, the majority of the sulfide minerals have $\delta^{34}S$ values peaking at −11 and −2‰. The $\delta^{34}S$ chalcopyrite values range from −11.6 to 1.1‰ (average −5.1‰), tetrahedrite has a variable $\delta^{34}S$ composition, ranging from −10 to 3.0‰ (average −1.3‰), and the $\delta^{34}S$ value for bornite is relatively heavy averaging 0.9‰.

6. Discussion

6.1. Ore-forming conditions

During the emplacement of the first vein sets at the Liancheng deposit, the mineralizing fluids included vapour-only, CO_2-rich, and liquid-rich fluid phases now preserved in quartz veins locally containing Cu sulfide. The fluid is characterized by middle- to high temperatures averaging ~250 °C and salinities averaging ~14 wt% NaCl equiv. The mineralizing fluid during the third and fourth hydrothermal events is represented by liquid-rich and liquid-only fluid inclusions observed in carbonate and carbonate-Cu sulfide veins. The late fluid is

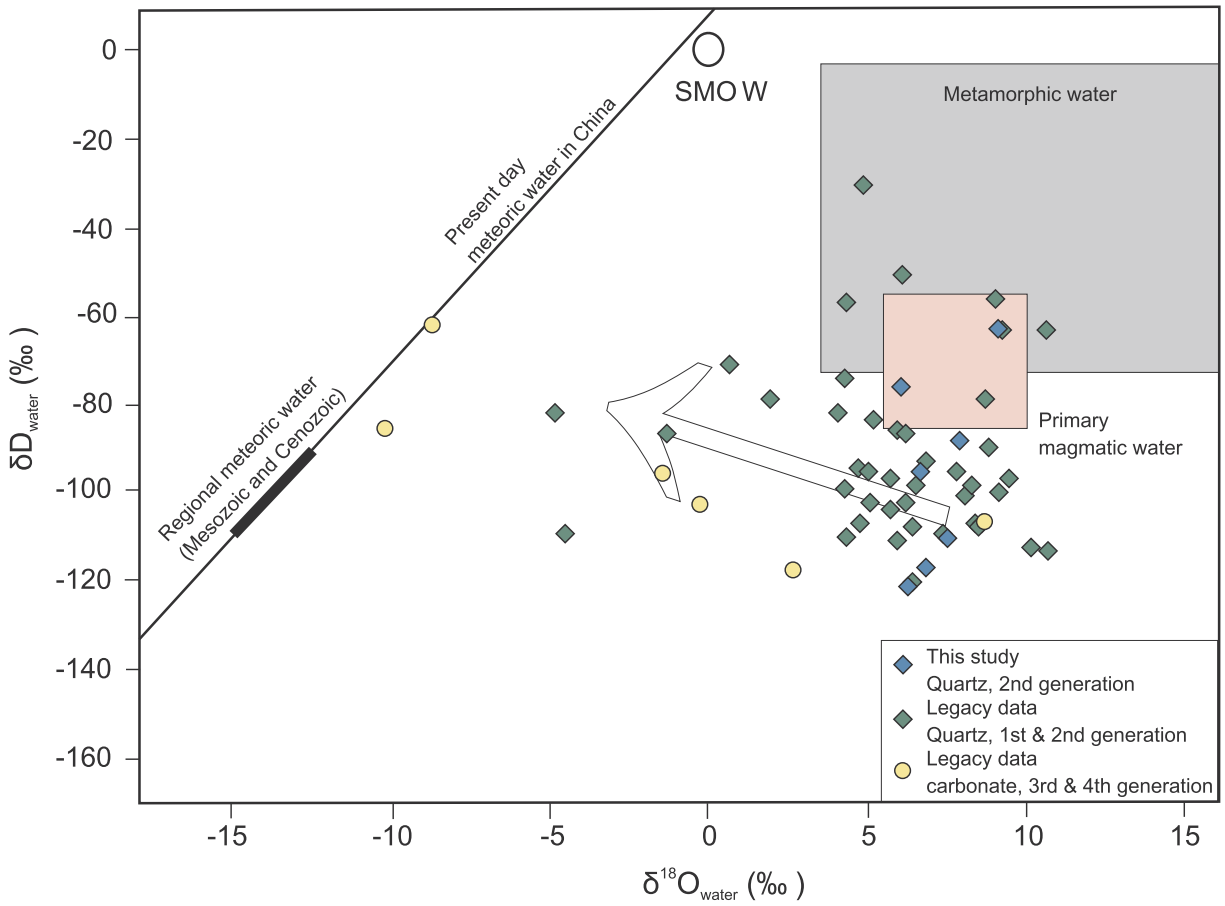

Fig. 10. Oxygen and hydrogen isotopic compositions, including published δD and $\delta^{18}O$ data from hydrothermal quartz and carbonate from the Liancheng Cu–Mo deposit. The regional meteoric water (Mesozoic and Cenozoic) is from Xu and Mo (2000). The present-day meteoric water in China is used for the composition of meteoric water (c.f. Xiao, 1989; Ji and Li, 1998; Liu et al., 2000; Chen and Wang, 2004; Zhao, 2006; Zhang et al., 2013; Song et al., 2016).

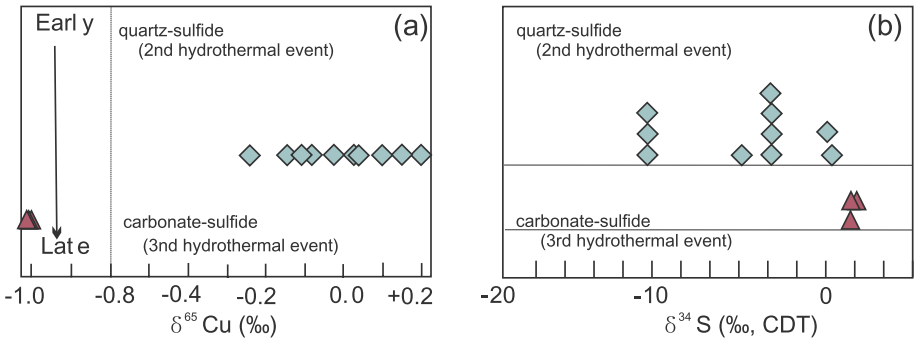

Fig. 11. Diagram showing the temporal-spatial distribution of sulfur and copper isotopes in sulfide minerals from the Liancheng Cu–Mo deposit: (a) Cu isotopes from different mineralization events; and (b) sulfur isotopes from different mineralization events.

characterized by lower temperature averaging 204 °C with a salinity averaging ~12 wt% NaCl equiv. The similar ranges of the salinity for each event indicate that the changes in salinity were not a key factor controlling Cu-sulfide precipitation in the Liancheng area (Figs. 8 and 9). Gradual changes are seen in the volume of CO_2 in the mineralizing fluid, which is represented by CO_2-rich fluid in the first two sets fluid inclusion, and the following two generations of fluid inclusions are not CO_2-rich. This decrease in CO_2 indicates that there was fluid mixing or boiling corresponding to decreases in pressure and temperature. This observation combined with the hydrogen and oxygen isotope analyses documented here indicate that the fluids were metamorphic in origin, with a minor input of meteoric water. Therefore, fluid mixing is not a critical factor in the deposition of Cu–Mo mineralization at Liancheng.

Several other processes, such as changes in redox state, fluid exsolution and biological effects can be factors resulting in the deposition of Cu-sulfides (e.g. Maréchal et al., 1999; Zhu et al., 2002; Larson et al., 2003; Markl et al., 2006; Qian et al., 2006; Asael et al., 2007; Fernandez and Borrok, 2009; Haest et al., 2009; Yang et al., 2016). Changes at the redox front from reducing to oxidising states can be a significant factor in whether Cu-sulfides remain in solution or precipitate (e.g. Rouxel et al., 2004; Mathur et al., 2005; Markl et al., 2006; Asael et al., 2007).

Copper (Cu) has two valences; Cu I (cuprous) has one valence electron and Cu II (cupric) has two valence electrons. The prominent Cu (I)-sulfide at Liancheng is chalcopyrite ($Cu^{I}Fe^{III}S_2$), and the minor Cu(I) bornite (between $Cu_5{}^{I}Fe^{III}S_4$ and $Cu_4{}^{I}Cu^{II}Fe^{II}S_4$) and tetrahedrite ($(Cu_{10}{}^{I}Cu_2{}^{II})As_4{}^{III}S_{13}$) are hosted by quartz in the early stages of mineralization. The late stages of mineralization are dominated by Cu(I)-sulfide minerals in tetrahedrite with minor Cu(I) bornite and chalcopyrite hosted by carbonate. It should be noted that despite contradictory views regarding the valency of copper in minerals such as

chalcopyrite and tetrahedrite, mineralogical studies at Liancheng have shown that copper coexists as the Cu(I) ion in different stages, indicating redox environments are unlikely significant controls for the composition of Cu isotopes in the Cu-sulfides (Boekema et al., 2004; Goh et al., 2006, 2010; Markl et al., 2006).

It is also noteworthy that the total range of δ^{65}Cu values at Liancheng is only ~1.3‰. If there were multiple Cu-mixing sources in the genesis of the deposit, it is unlikely that only a narrow range of δ^{65}Cu would exist at the deposit (Asael et al., 2005; Mathur et al., 2005). Therefore, fluid mixing does not account for the limited range in the Cu-isotope composition observed at Liancheng, which largely reflects a homogenous source.

Markl et al. (2006) proposed that the pH of an acidic mineralized fluid will increase when it reacts with carbonate rocks, which results in the deposition of Cu minerals at near-neutral pH, which is a process that can drive kinetic isotopic fractionation. It is therefore proposed that such a reaction at Liancheng would have resulted in an increase in the pH of the mineralizing fluid from a value of ~6 to over 7, and the pH increase could have been the primary control on the limited Cu-isotope variation (Zhao, 2006). The late stage Cu minerals accompanied by carbonate in the ore displays the clearest evidence for this pH driven kinetic isotope fraction of δ^{65}Cu. The high copper isotopic data for the quartz-Cu sulfide ore is related to the relative high temperatures during the early stages of mineralization, and light copper isotopic data for the carbonate-Cu mineral with relative low temperature in the late stages of the mineralization (with a positive correlation of $r^2 = 0.89$) (Tables 1 and 2). The small variation in δ^{65}Cu values for sulfides at Liancheng indicates that a variation in temperature was an important control on the composition of Cu isotopes in Cu minerals. Thus, the dominant processes controlling the Cu isotope variability at Liancheng are probably largely the temperature and pH of the mineralizing fluid.

6.2. Ore-forming fluids for the Cu–Mo mineralization

The $\delta^{18}O_{H2O}$ values of the mineralizing fluids are calculated using the homogenisation temperatures of primary fluid inclusions and the quartz-water equilibrium fractionation of Clayton et al. (1972). The $\delta^{18}O_{H2O}$ values in the early stages of the hydrothermal fluids overlap in the magmatic and metamorphic fields shown in Fig. 11. In addition, the H and O isotopic compositions can be interpretation as being related dominated to metamorphic waters with addition of magmatic water. Zhang et al. (2015) conclude that noble gas isotope compositions have no characteristic indicative of a mantle fluid involvement for the Liancheng deposit. Based on the lack of coeval igneous rocks in the Lanping Basin, metamorphic water components seem to be a likely source for the CO_2-rich fluid. Furthermore, compared to the early stage fluids, the later stage fluids slightly shift toward the composition of meteoric water, indicating that the fluids do have a meteoric component for the later hydrothermal event.

6.3. Sources of metals

The mantle, magma, and country rocks have been proposed as sources for the sulfur at Liancheng (Xiao et al., 1994; Ji and Li, 1998; Yan and Li, 1997; Liu et al., 2000; Wu et al., 2003; Song et al., 2016). Zhang et al. (2015) suggest that the source was derived from a mixed sedimentary and magma deep in the crust. In this contribution, the bimodal δ^{34}S values of −4.8 to 3.0‰ and −10 to −11.5‰ of sulfides from Liancheng can be interpreted as having a sulfur source from magmatic, mantle-derived, or metamorphic fluids (Table 4; c.f. Ohmoto and Rye, 1979; Goldfarb et al., 2005).

The ages of the Cu-Mo mineralization have been reported using different dating methods, such as molybdenite Re–Os (47.8 ± 1.8 Ma and 48.14 ± 0.87 Ma), quartz $^{40}Ar/^{39}Ar$ (58. 05 ± 0. 54 Ma and 56.7 ± 1 Ma), calcite Sm–Nd (58.2 ± 5.3 Ma), and apatite fission track thermochronometry (46.1 ± 5.8 Ma) (Liu et al., 2003; Xu et al., 2004; Li and Song, 2006; Wang, 2010; Zhang et al., 2013). There is no indication of a magmatic event was present in the basin during the mineralizing event. The only magmatic rocks present in the Lanping Basin are Middle to Late Triassic (ca. 235 to 210 Ma) mafic and felsic volcanic sequences and Middle Eocene to Early Oligocene (ca. 41 to 32 Ma) potassic to ultra potassic magmatic rocks along the basin's margins (Deng et al. 2014a,b; Wang et al. 2014b). Furthermore, metamorphic age of 49 Ma, corresponding to ore-forming age of the Liancheng deposit, is documented in the region (Gong et al., 2006). This points to the Lanping Basin being tectonically active during the India-Asia continental collision, which provided the driving force for the concentration of metamorphic fluids (Wang et al., 2017a).

In addition, a mantle-derived source has been ruled out by noble gas isotope compositions for the Liancheng deposit (Zhang et al., 2015). Thus, it is considered very likely that the sulfur at the Liancheng deposit has a mantle or a magmatic source. Samples of tetrahedrite and chalcopyrite from the Liancheng block have δ^{34}S values of −10 to −11.5‰, which are higher than those from the Jinding MVT deposit (Deng et al., 2016). Earlier studies have also proposed that sulfur with moderate negative δ^{34}S values at Liancheng originate from sulfur reduction by bacteria (Yang et al., 2016). However, the fluid inclusion homogenisation temperatures in the ore-forming second and third hydrothermal events are between 124 and 407 °C. This temperature range is too high for bacterial sulfate reduction and bacteriogenic sulfur being produced from the sedimentary country rocks (c.f. Machel et al., 1995; Warren, 2000; Machel, 2001; Kashefi and Lovley, 2003; Deng et al., 2016). In addition, the δ^{34}S values at Liancheng are consistent with sulfur being derived from a deeper source below the basin's floor.

Table 4
Geological characteristics comparison between the Liancheng Cu–Mo deposit and orogenic type deposits.

Typical characteristics	Orogenic gold deposits	Shagou Ag–Pb–Zn deposit	West Carbery Cu deposit	Liancheng Cu–Mo deposit
Tectonic setting	Orogenic belt	Qinling collisional orogenic belt, China	Orogenic belt, Ireland	Sanjiang orogenic belt, China
Host rock	Mainly metamorphic rocks, and other rock types	Metamorphic Taihua Group	Metasedimentary rocks	Metasedimentary rocks, with metamorphic basement
Metamorphic grade of host rocks	Mainly greenschist facies but subgreenschist to lower granulite facies	Gneiss and amphibolite	Metamorphosed to slate	Metamorphosed to slate and schist
Ore-controlling structure	Structurally-controlled	Structurally-controlled	No	Structurally-controlled
Mineralization style	Veins, breccias, disseminated	Quartz veins	Quartz veins and veinlets	Quartz or carbonate veins
Alteration types	Carbonate, sericite, silica, albite, tourmaline	Carbonate, sericite, silica	Carbonate, sericite, silica, chlorite, albite	Carbonate, sericite, ankerite, and minor graphite
Ore mineral assemblages	Pyrite, arsenopyrite, stibnite	Pyrite, sphalerite, galena and Ag-bearing sulfides	Chalcopyrite, bornite, chalcocite	Chalcopyrite, tetrahedrite, bornite, tennantite
Fluid source	Metamorphic fluids	Metamorphic fluids	Metamorphic fluids	Metamorphic fluids
Temperature	220–600 °C	180–220 °C	280–350 °C	124–466 °C
References	Goldfarb et al. (2005)	Han et al. (2014)	Wen et al. (1996)	This study

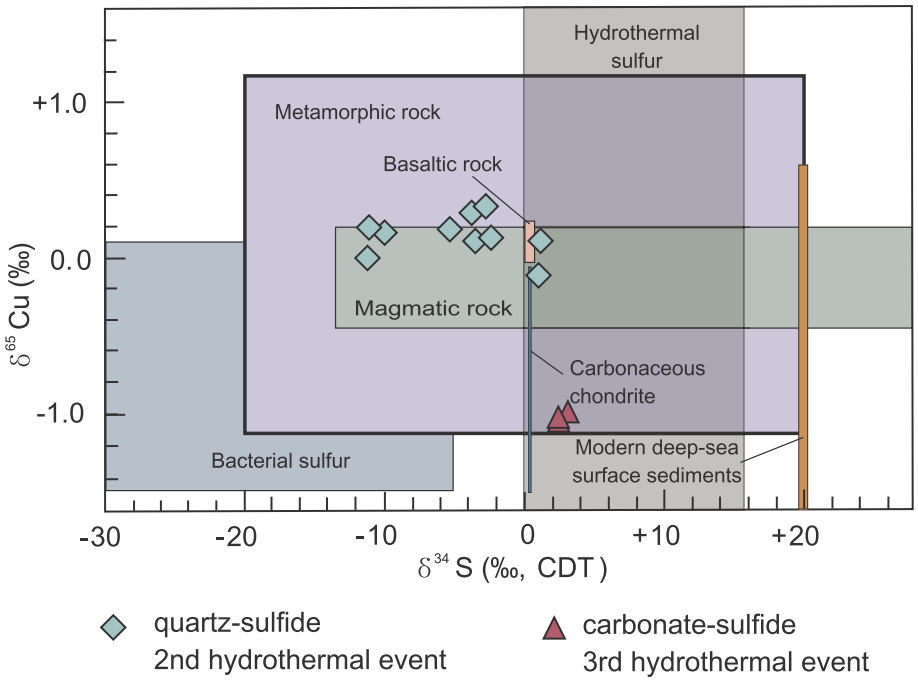

Fig. 12. Plot of $\delta^{34}S_{CDT}$ vs $\delta^{65}Cu$. The Cu isotope composition is plotted as a function of the Cu-sulfur isotope composition from the same sample. Boxes show the compositions of sphalerite where hydrothermal and bacteriogenic fluids are proposed to dominate. Boxes show compositions of $\delta^{65}Cu$ and $\delta^{34}S_{CDT}$ as follows: carbonaceous chondrite ($\delta^{65}Cu = -1.51$ to -0.03‰ and $\delta^{34}S_{CDT} = 0.4$‰); basalt rocks ($\delta^{65}Cu = -0.01$ to $+0.22$‰ and $\delta^{34}S_{CDT} = \pm 1$‰); magmatic rocks ($\delta^{65}Cu = -0.46$ to $+0.21$‰ and $\delta^{34}S_{CDT} = -13.4$ to $+28.7$‰); metamorphic rocks ($\delta^{65}Cu = -1.1$ to $+1.2$‰ and $\delta^{34}S_{CDT} = -20$ to $+20$‰); modern deep sea surface sediments ($\delta^{65}Cu = -2.83$ to $+0.6$‰ and $\delta^{34}S_{CDT} = +20$‰); hydrothermal sulfur ($\delta^{65}Cu = -3.7$ to $+2.98$‰ and $\delta^{34}S_{CDT} > 0$‰); and bacteriogenic sulfur ($\delta^{65}Cu = -1.50$ to $+0.62$‰ and $\delta^{34}S_{CDT} = < -5$‰) (Thode et al., 1961; Maréchal et al., 1999; Zhu et al., 2000; Maréchal and Albarède, 2002; Ben et al., 2003; Larson et al., 2003; Luck et al., 2003, 2005; Albarède, 2004; Archer and Vance, 2004; Ehrlich et al., 2004; Graham et al., 2004; Rouxel et al., 2004; Mason et al., 2005; Mathur et al., 2005; Markl et al., 2006; Asael et al., 2007; Maher and Larson, 2007; Moynier et al., 2007, 2010; Haest et al., 2009; Herzog et al., 2009; Li et al., 2009, 2010; Mathur et al., 2009; Wang and Zhu, 2010; Bigalke et al., 2011; Navarrete et al., 2011; Weinstein et al., 2011; Liu et al., 2014).

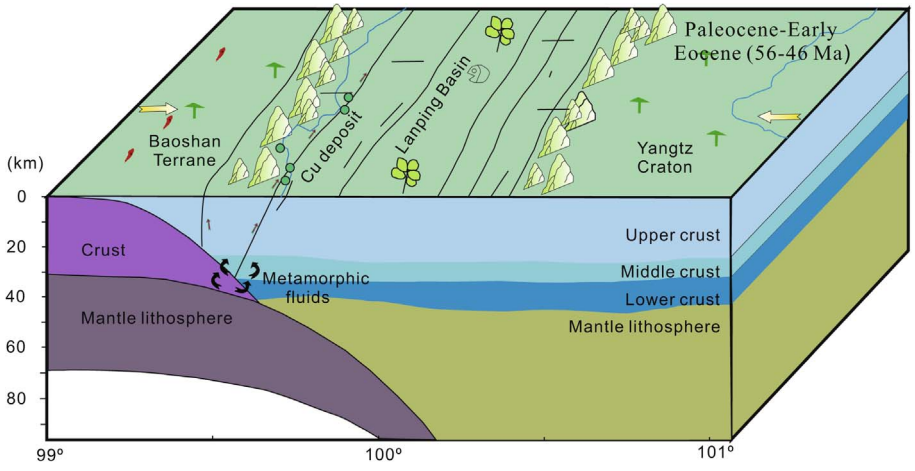

Fig. 13. Tectonic model for the Liancheng Cu–Mo deposit.

The $\delta^{65}Cu$ values for the quartz-Cu sulfides at Liancheng range from -0.31 to 0.2‰, but Cu-sulfide mineralization associated with carbonate (hydrothermal event 3) ranges from -1.01 to -1.08‰. The quartz-Cu sulfide samples from the earlier mineralization event (2) have a similar pattern.

Samples with isotopically light Cu from the later stage of the carbonate-Cu sulfide mineralization have a source that is difficult to pinpoint, because the copper isotopic values overlap the magmatic fields with $\delta^{65}Cu$ between -0.62 and $+0.4$‰, VMS deposits with $\delta^{65}Cu$ from 0.62 to $+0.34$‰, porphyry and skarn deposits with $\delta^{65}Cu$ between -1.29 and $+2.98$‰, hydrothermal vein type deposits with $\delta^{65}Cu$ between -3.7 and $+2.41$‰, and sedimentary deposits with $\delta^{65}Cu$ values between -2.54 and -0.66‰ (c.f., Maréchal et al., 1999; Zhu et al., 2000; Larson et al., 2003; Graham et al., 2004; Mason et al., 2005; Markl et al., 2006; Asael et al., 2007; Maher and Larson, 2007; Mathur et al., 2009).

The coupling of Cu and S isotopic fractionation provides indications of the likely source of the copper at Liancheng (Zhou et al., 2013; Molnár et al., 2016). The plot in Fig. 12 indicates that copper is derived from metamorphic rocks. Furthermore, the measured $\delta^{65}Cu$ compositions of the Cu sulfides are similar to those sourced from metamorphic rocks worldwide. See Fig. 13

6.4. Ore genesis

The age of the Cu–Mo mineralization at Liancheng is Paleocene to Early Eocene, which coincides with the collision of the Indian and Asian continents (Wang et al., 2017a). Most of the mineralization in the Lanping Basin is located in NNE-trending reverse faults, and associated shears and tensile fractures in the upper member of the Huakaizuo Formation (Fig. 3), which are features different from examples of sediment-hosted stratiform Cu deposits on Earth (Brown, 1978, 1997; Leach et al., 2005).

In order to better constrain the genesis of the Liancheng Cu–Mo deposit, geological and fluid characteristics among orogenic gold belts and orogenic Pb–Zn–Cu–Ag deposits are compared with those of the Liancheng deposit in Table 4. These characteristics are similar for the three types of deposits indicating a similar genesis (Table 4). Therefore, the presented data and discussion here indicates that the Liancheng Cu–Mo deposit is orogenic, with examples know at the West Carbery Cu

deposits in Ireland, and the Qinling Pb–Zn–Cu–Ag deposit in China (Wen et al., 1996; Chen et al., 2004; Zhang et al., 2013; Han et al., 2014).

7. Conclusions

The Paleocene-Early Eocene Liancheng deposit formed during the collision of the India and Asia continents. The richest Cu–Mo mineralization at the deposits is located in quartz-sulfide and carbonate-sulfide veins that are hosted by layer-parallel shear zones at Liancheng. Hydrogen and oxygen isotopes from mineralized quartz-sulfide and carbonate-sulfide veins indicate that the ore-forming fluid is largely from metamorphic water, with a minor contribution from meteoric water. The copper and sulfur isotope geochemistry indicates that the source of the mineralization is rocks underneath the basin, and the factors controlling the deposition of the mineralization are principally temperature, pressure, and pH. We propose that the Liancheng Cu–Mo deposit is orogenic in type and deposited in a sedimentary basin during the Paleocene-Early Eocene collision of the India and China plates.

Acknowledgements

This research is jointly supported by the National Basic Research Program of China (Projects 2015CB452603 and 2009CB421008), the Fundamental Research Funds for the Central Universities of China (Projects 2652016077, 2652017223), and the 111 Project (Project B07011). We thank Professors Yan Tao and Yinhong Wang for their valuable help and the anonymous referees for their helpful comments improving the manuscript.

References

Albarède, F., 2004. The stable isotope geochemistry of copper and zinc. Rev. Mineral. Geochem. 55, 409–427.
Archer, C., Vance, D., 2004. Mass discrimination correction in multiple-collector plasma source mass spectrometry an example using Cu and Zn isotopes. J. Anal. At. Spectrom. 19, 656–665.
Asael, D., Matthews, A., Bar-Matthews, M., Halicz, L., Ehrlich, S., Teplyakov, N., 2005. Redox fractionation of copper isotopes in sedimentary conditions. Geochim. Cosmochim. Acta 69, A216.
Asael, D., Matthews, A., Oszczepalski, S., Bar-Matthews, M., Halicz, L., 2007. Copper isotope fractionation in sedimentary copper mineralisation (Timna Valley, Israel). Chem. Geol. 243, 238–254.
Baumgartner, R., Fontboté, L., Vennemann, T., 2008. Mineral zoning and geochemistry of epithermal polymetallic Zn–Pb–Ag–Cu–Bi mineralisation at Cerro de Pasco, Peru. Econ. Geol. 103, 493–537.
Beaudoin, G., Sangster, D.F., 1992. A descriptive model for silver-lead zinc veins in clastic metasedimentary terranes. Econ. Geol. 87, 1005–1021.
Ben, O.D., Luck, J.M., Tchalikian, J.M., Albarède, F., 2003. Cu–Zn isotope systematics in terrestrial basalts. Geophysical. Res. Abstracts 5, 9669.
Bendezú, R., Fontboté, L., Cosca, M., 2003. Relative age of Cordilleran base metal lode and replacement deposits, and high sulfidation Au-(Ag) epithermal mineralisation in the Colquijirca mining district, central Peru. Miner. Deposita 38, 683–694.
Bi, X.M., Mo, X.X., 2004. Transition from diagenesis to low-grade metamorphism and related minerals and energy resources. Earth Sci. Front. 11, 287–294 (in Chinese with English abstract).
Bigalke, M., Weyer, S., Wilcke, W., 2011. Stable Cu isotope fractionation in soils during oxic weathering and podzolization. Geochim. Cosmochim. Acta 75, 3119–3134.
Bodnar, R.J., 1993. Revised equation and table for determining the freezing point depression of H_2O-NaCl solutions. Geochim. Cosmochim. Acta 57, 683–684.
Boekema, C., Mkrupski, A., Varasteh, M., Parvin, K., van Til, F., van der Woude, F., Sawatzky, G.A., 2004. Cu and Fe valence states in $CuFeS_2$. J. Magn. Magn. Mater. 272–276, 559–561.
Brown, A.C., 1978. Stratiform copper deposits—evidence for their post-sedimentary origin. Miner. Sci. Eng. 10, 172–181.
Brown, A.C., 1997. World-class sediment-hosted stratiform copper deposits: characteristics, genetic concepts and metallotects. Aust. J. Earth Sci. 44, 317–328.
Chen, J., Wang, H., 2004. Geochemistry. Science Press, Beijing, pp. 129 (in Chinese).
Chen, Y.J., Pirajno, F., Sui, Y.H., 2004. Isotope geochemistry of the Tieluping silver-lead deposit, Henan, China: a case study of orogenic silver-dominated deposits and related tectonic setting. Miner. Deposita 39, 560–575.
Chi, G.X., Xue, C.J., 2011. Abundance of CO_2-rich fluid inclusions in a sedimentary basin-hosted Cu deposit at Jinman, Yunnan, China: implications for mineralisation environment and classification of the deposit. Miner. Deposita 46, 365–380.
Clayton, R.N., O'Neil, J.R., Mayeda, T.K., 1972. Oxygen isotope exchange between quartz and water. J. Geophys. Res. 77, 3057–3067.
Collins, P.L.F., 1979. Gas hydrates in CO_2-bearing fluid inclusions and the use of freezing date for estimation of salinity. Econ. Geol. 74, 1435–1444.
Deng, J., Wang, Q.F., Li, G.J., Li, C.S., Wang, C.M., 2014a. Tethys tectonic evolution and its bearing on the distribution of important mineral deposits in the Sanjiang region, SW China. Gondwana Res. 26, 419–437.
Deng, J., Wang, Q.F., Li, G.J., Santosh, M., 2014b. Cenozoic tectono-magmatic and metallogenic processes in the Sanjiang region, southwestern China. Earth-Sci. Rev. 138, 268–299.
Deng, J., Wang, C.M., Bagas, L., Carranza, E.J.M., Lu, Y.J., 2015a. Cretaceous-Cenozoic tectonic history of the Jiaojia Fault and gold mineralisation in the Jiaodong Peninsula, China: Constraints from zircon U-Pb, illite K–Ar, and apatite fission track thermochronometry. Miner. Deposita 50, 987–1006.
Deng, J., Wang, Q.F., Li, G.J., Hou, Z.Q., Jiang, C.Z., Danyushevsky, L., 2015b. Geology and genesis of the giant Beiya porphyry-skarn gold deposit, northwestern Yangtze Block, China. Ore Geol. Rev. 70, 457–485.
Deng, J., Wang, C.M., Bagas, L., Selvaraja, V., Jeond, H., Wu, B., Yang, L., 2016. Insights into ore genesis of the Jinding Zn–Pb deposit, Yunnan Province, China: evidence from Zn and in-situ S isotopes. Ore Geol. Rev. https://doi.org/10.1016/j.oregeorev.2016.10.036.
Deng, J., Wang, Q.F., Li, G.J., 2017. Tectonic evolution, superimposed orogeny, and composite metallogenic system in China. Gondwana Res. 50, 216–266.
Driesner, T., Heinrich, C.A., 2007. The system H_2O-NaCl. Part I: correlation formulae for phase relations in temperature-pressure-composition space from 0 to 1000°C, 0 to 5000 bar, and 0 to 1 X_{NaCl}. Geochim. Cosmochim. Acta 71, 4880–4901.
Du, B., Wang, C.M., He, X.Y., Yang, L.F., Chen, J.Y., Shi, K.X., Luo, Z., Xia, J.S., 2016. Advances in research of bulk-rock Nd and zircon Hf isotopic mappings: case study of the Sanjiang Tethyan Orogen. Acta Petrol. Sin. 32, 2555–2570 (in Chinese with English abstract).
Dupont-Nivet, G., Lippert, P.C., van Hinsbergen, D.J., Meijers, M.J., Kapp, P., 2010. Palaeolatitude and age of the Indo-Asia collision: palaeomagnetic constraints. Geophys. J. Inter. 182, 1189–1198.
Ehrlich, S., Butler, I., Halicz, L., Rickard, D., Oldroyd, A., Matthews, A., 2004. Experimental study of the copper isotope fractionation between aqueous Cu(II) and covellite, CuS. Chem. Geol. 209, 259–269.
Fan, J.W., Yang, T.N., Liang, M.J., Shi, P.L., 2014. LA-ICP-MS zircon U–Pb geochronology and geochemistry of volcanic rocks on the western margin of Lanping Basin in western Yunnan and their tectonic implications. Acta Petrol. Mineral. 33, 471–490 (in Chinese with English abstract).
Fernandez, A., Borrok, D.M., 2009. Fractionation of Cu, Fe, and Zn isotopes during the oxidative weathering of sulfide-rich rocks. Chem. Geol. 264, 1–12.
Gao, Z.Q., Zhao, Q.H., Tong, Y.H., 2006. Jinman sedimentation hydrothermal reformation Cu deposit, Lanping. J. Yunnan Geol. 25, 3–7 (in Chinese with English abstract).
Germann, K., Lüders, V., Banks, D.A., Simon, K., Hoefs, J., 2003. Late Hercynian polymetallic vein-type base-metal mineralisation in the Iberian pyrite belt: fluid-inclusion and stable-isotope geochemistry (S–O–H–Cl). Miner. Deposita 38, 953–967.
Goh, S.W., Buckley, A.N., Lamb, R.N., Rosenberg, R.A., Moran, D., 2006. The oxidation states of copper and iron in mineral sulfides, and the oxides formed on initial exposure of chalcopyrite and bornite to air. Geochim. Cosmochim. Acta 70, 2210–2228.
Goh, S.W., Buckley, A.N., Skinner, W.M., Fan, L.J., 2010. An X-ray photoelectron and absorption spectroscopic investigation of the electronic structure of cubanite, $CuFe_2S_3$. Phys. Chem. Miner. 37, 389–405.
Goldfarb, R., Baker, T., Dube, B., Groves, D.I., Hart, C.J.R., Gosselin, P., 2005. Distribution, character and genesis of gold deposits in metamorphic terranes. Econ. Geol. 407–450 100th Anniversary Volume.
Gong, J.F., Ji, J.Q., Sang, H.Q., Han, B.F., Li, B.L., Chen, J., J, 2006. $^{40}Ar/^{39}Ar$ geochronology of high-pressure granulite xenolith and its surrounding granite in central Himalaya. Acta Petrol. Sin. 22, 2677–2686 (in Chinese with English abstract).
Graham, S., Pearson, N., Jackson, S., Griffin, W., O'Reilly, S.Y., 2004. Tracing Cu and Fe from source to porphyry: in situ determination of Cu and Fe isotope ratios in sulfides from the Grasberg Cu–Au deposit. Chem. Geol. 207, 147–169.
Haest, M., Muchez, P., Petit, J.C.J., Vanhaecke, F., 2009. Cu isotope ratio variations in the Dikulushi Cu–Ag deposit, DRC: of primary origin or induced by supergene reworking? Econ. Geol. 104, 1055–1064.
Han, J.S., Yao, J.M., Chen, H.Y., Deng, X.H., Ding, J.Y., 2014. Fluid inclusion and stable isotope study of the Shagou Ag–Pb–Zn deposit, Luoning, Henan province, China: implications for the genesis of an orogenic lode Ag–Pb–Zn system. Ore Geol. Rev. 62, 199–210.
Herzog, G.F., Moynier, F., Albarède, F., Berezhnoy, A.A., 2009. Isotopic and elemental abundances of copper and zinc in lunar samples, Zagami, Pele's hairs, and a terrestrial basalt. Geochim. Cosmochim. Acta 73, 5884–5904.
Hitzman, M., Kirkham, R., Broughton, D., Thorson, J., Selley, D., 2005. The sediment-hosted stratiform copper ore system. Econ. Geol. 609–642 100th Anniversary Volume.
Hou, Z.Q., Song, Y.C., Li, Z., Wang, Z.L., Yang, Z.M., Yang, Z.S., Liu, Y.C., Tian, S.H., He, L.Q., Chen, K.X., Wang, F.C., Zhao, C.X., Xue, W.W., Lu, H.F., 2008. Thrust-controlled, sediments–hosted Pb–Zn–Ag–Cu deposits in eastern and northern margins of Tibetan orogenic belt: geological features and tectonic model. Mineral Deposits 27, 123–144 (in Chinese with English abstract).
Huang, S.Q., Song, Y.C., Hou, Z.Q., Xue, C.D., 2016. Chemical and stable isotopic (B, H, and O) compositions of tourmaline in the Maocaoping vein-type Cu deposit, western Yunnan, China: Constraints on fluid source and evolution. Chem. Geol. 439, 173–188.
Ji, H.B., Li, C.Y., 1998. Geochemistry of Jinman copper vein deposit, west Yunnan Province, China: fluid inclusion and stable isotope geochemical characteristics. Chin. J. Geochem. 17, 81–90.
Kashefi, K., Lovley, D.R., 2003. Extending the upper temperature limit for life. Science 301, 934.

Larson, P.B., Maher, K., Ramos, F.C., Chang, Z., Gaspar, M., Meinert, L.D., 2003. Copper isotope ratios in magmatic and hydrothermal ore-forming environments. Chem. Geol. 201, 337–350.
Leach, D.L., Sangster, D.F., Kelley, K.D., Large, R.R., Garven, G., Allen, C., Gatzmer, J., Wallters, S., 2005. Sediment-hosted lead-zinc deposit: a global perspective. Econ. Geol. 561–607 100th Anniversary Volume.
Lecumberri-Sanchez, P., Steele-MacInnis, M., Bodnar, R.J., 2012. A numerical model to estimate trapping conditions of fluid inclusions that homogenize by halite disappearance. Geochim. Cosmochim. Acta 92, 14–22.
Li, F., Fu, W.M., 2000. Geology of Red Beds Copper Deposits in Western Yunnan. Yunnan University of Publishing House, Kunming, pp. 60 (in Chinese).
Li, X.M., Song, Y.G., 2006. Cenozoic evolution of tectono-fluid and metallogenic process in the Lanping Basin, western Yunnan Province, Southwest China: constraints from apatite fission track data. Chin. J. Geochem. 15, 405–408.
Li, F., Fu, W.M., Ran, C.Y., Zhou, Z.M., Zhao, Z.B., Lu, W.J., 1993. Geological and geochemical characteristics of Jinman Copper deposit in Lanping County, Yunnan Province. Mineral Resour. Geol. 7, 176–182 (in Chinese with English abstract).
Li, F., Fu, W.M., Li, L., 1997. Sources of ore-forming material for regional red-bed copper mineralisation in western Yunnan. Geol. Yunnan 3, 233–244 (in Chinese with English abstract).
Li, W., Jackson, S.E., Pearson, N.J., Alard, O., Chappell, B.W., 2009. The Cu isotopic signature of granites from the Lachlan Fold Belt, SE Australia. Chem. Geol. 258, 38–49.
Li, W., Jackson, S.E., Pearson, N.J., Graham, S., 2010. Copper isotopic zonation in the Northparkes porphyry Cu–Au deposit, SE Australia. Geochim. Cosmochim. Acta 74, 4078–4096.
Liang, H.Y., Campbell, I.H., Allen, C.M., Sun, W.D., Yu, H.X., Xie, Y.W., Zhang, Y.Q., 2007. The age of the potassic alkaline igneous rocks along the Ailaoshan-Red River Shear Zone: implications for the onset age of left-lateral shearing. J. Geol. 115, 231–242.
Liang, H.Y., CampbelI, H., Allen, C.M., Sun, W.D., Xie, Y.W., Zhang, Y.Q., 2008. The Age of the potassic alkaline igneous rocks along the Ailaoshan-Red River shear zone: implications for the onset age of left–lateral shearing: a reply. J. Geol. 116, 205–207.
Liang, M.J., Yang, T.N., Shi, P.L., Xue, C.D., Xiang, K., Liao, C., 2015. U-Pb geochronology, Hf isotopes of zircons from the volcanic rocks along the eastern margin of Lanping basin, Sanjiang orogenic belt. Acta Petrol. Sin. 31, 3247–3268 (in Chinese with English abstract).
Liu, J.J., Li, C.Y., Pan, J.Y., Liu, X.F., Zhang, Q., Liu, Y.P., 2000. Ore-forming material sources of the copper deposits from sandstone and shale in Lanping-Simao Basin, western Yunnan and their genetic implications. Geol. Prospect. 36, 16–19 (in Chinese with English abstract).
Liu, J.J., Li, Z.M., Zhang, Q., Liu, Y.P., Li, C.Y., He, M., Sang, H.Q., Yang, W.G., Yang, A.P., 2002. $^{40}Ar/^{39}Ar$ fast neutron activation ages of quartz from the Jinman vein copper deposit in western Yunnan and their significance. Chin. J. Geochem. 21, 227–233.
Liu, J.J., Li, Z.M., Liu, Y.P., Li, C.Y., Zhang, Q., He, M.Q., Yang, W.G., Yang, A.P., Sang, H.Q., 2003. The metallogenic age of Jinman vein copper deposit, Western Yunnan. Geoscience 17, 34–39 (in Chinese with English abstract).
Liu, S.A., Li, D.D., Li, S.G., Teng, F.Z., Ke, S., He, Y.S., Lu, Y.H., 2014. High-precision copper and iron isotope analysis of igneous rock standards by MC-ICP-MS. J. Anal. At. Spectrom. 29, 122–133.
Lu, Y.J., Kerrich, R., Cawood, P.A., McCuaig, T.C., Hart, C.J.R., Li, Z.X., Hou, Z.Q., Bagas, L., 2012. Zircon SHRIMP U-Pb geochronology of potassic felsic intrusions in western Yunnan, SW China: constraints on the relationship of magmatism to the Jinsha suture. Gondwana Res. 22, 737–747.
Lu, Y.J., Kerrich, R., Kemp, A.I.S., McCuaig, T.C., Hou, Z.Q., Hart, C.J.R., Li, Z.X., Cawood, P.A., Bagas, L., Yang, Z.M., Cliff, J., Belousova, E.A., Jourdan, F., Evans, N.J., 2013. Intracontinental Eocene-Oligocene porphyry Cu mineral systems of Yunnan, western Yangtze Craton, China: compositional characteristics, sources, and implications for continental collision metallogeny. Econ. Geol. 108, 1541–1576.
Luck, J.M., Othman, D.B., Barrat, J.A., Albarède, F., 2003. Coupled ^{63}Cu and ^{16}O excesses in chondrites. Geochim. Cosmochim. Acta 67, 143–151.
Luck, J.M., Ben, O.D., Albarède, F., 2005. Zn and Cu isotopic variations in chondrites and iron meteorites: early solar nebula reservoirs and parent- body processes. Geochim. Cosmochim. Acta 69, 5351–5363.
Machel, H.G., 2001. Bacterial and thermochemical sulfate reduction in diagenetic settings: old and new insights. Sediment. Geol. 140, 143–175.
Machel, H.G., Krouse, H.R., Sassen, R., 1995. Products and distinguishing criteria of bacterial and thermochemical sulfate reduction. Appl. Geochem. 10, 373–389.
Maher, K.C., Larson, P.B., 2007. Variation in copper isotope ratios and controls on fractionation in hypogene skarn mineralisation at Coroccohuayco and Tintaya. Perú. Econ. Geol. 102, 225–237.
Maréchal, C., Albarède, F., 2002. Ion-exchange fractionation of copper and zinc isotopes. Geochim. Cosmochim. Acta 66, 1499–1509.
Maréchal, C.N., Télouk, P., Albarède, F., 1999. Precise analysis of copper and zinc isotopic compositions by plasma-source mass spectrometry. Chem. Geol. 156, 251–273.
Markl, G., Lahaye, Y., Schwinn, G., 2006. Copper isotopes as monitors of redox processes in hydrothermal mineralisation. Geochim. Cosmochim. Acta 70, 4215–4228.
Mason, T.F.D., Weiss, D.J., Chapman, J.B., Wilkinson, J.J., Tessalina, S.G., Spiro, B., 2005. Zn and Cu isotopic variability in the Alexandrinka volcanic-hosted massive sulphide (VHMS) ore deposit, Urals. Russia. Chem. Geol. 221, 170–187.
Mathur, R., Ruiz, J., Titley, S., Liermann, L., Buss, H., Brantley, S., 2005. Cu isotopic fractionation in the supergene environment with and without bacteria. Geochim. Cosmochim. Acta 69, 5233–5246.
Mathur, R., Titley, S., Barra, F., Brantley, S., Wilson, M., Phillips, A., 2009. Exploration potential of Cu isotope fractionation in porphyry copper deposits. J. Geochem. Explor. 102, 1–6.
Molnár, F., Mänttäri, I., O'Brien, H., Lahaye, Y., Pakkanen, L., Johanson, B., Käpyaho, A., Sorjonen-Ward, P., Whitehouse, M., Sakellaris, G., 2016. Boron, sulphur and copper isotope systematics in the orogenic gold deposits of the Archaean Hattu schist belt, eastern Finland. Ore Geol. Rev. 77, 133–162.
Moynier, F., Blichert-Toft, J., Telouk, P., Luck, J.M., Albarède, F., 2007. Comparative stable isotope geochemistry of Ni, Cu, Zn, and Fe in chondrites and iron meteorites. Geochim. Cosmochim. Acta 71, 4365–4379.
Moynier, F., Koeberl, C., Beck, P., Jourdan, F., Telouk, P., 2010. Isotopic fractionation of Cu in tektites. Geochim. Cosmochim. Acta 74, 799–807.
Navarrete, J.U., Borrok, D.M., Viveros, M., Ellzey, J.T., 2011. Fractionation of Cu isotopes during adsorption and intracellular incorporation by bacteria. Geochim. Cosmochim. Acta 75, 784–799.
Ohmoto, H., Rye, R., 1979. Isotopes of sulfur and carbon. In: Barnes, H.L. (Ed.), Geochemistry of Hydrothermal Ore Deposits. John Wiley, New York, pp. 509–576.
Polliand, M., Moritz, R., 1999. Basement-hosted quartz-barite sulfide veins in the French Alps: a record of alpine tectonic fluid expulsion in the external crystalline massifs, structural, fluid inclusion, and isotope (S and Sr) evidences. Econ. Geol. 94, 37–56.
Qian, P., Lu, J.J., Liu, F.X., 2006. Isotopic tracing of ore-forming source materials in the porphyry copper deposit of Dexing, Jiangxi Province. Global Geol. 25, 135–140 (in Chinese with English abstract).
Que, M.Y., Chen, D.M., Zhang, L.S., Xia, W.J., Zhu, C.Y., 1998. Copper Deposits in Lanping and Simao Basin. Geological Publishing House, Beijing, pp. 109 (in Chinese).
Roedder, E., 1984. Fluid inclusions. Rev. Mineral. 12, 644p.
Rouxel, O., Fouquet, Y., Ludden, J.N., 2004. Copper isotope systematics of the Lucky Strike, Rainbow, and Logatchev sea-floor hydrothermal fields on the Mid-Atlantic Ridge. Econ. Geol. Bull. Soc. Econ. Geol. 585–600.
Song, Y., Hou, Z., Cheng, Y., Yang, T.N., Xue, C., 2016. Fluid inclusion and isotopic constraints on the origin of ore-forming fluid of the Jinman-Liancheng vein Cu deposit in the Lanping Basin, western Yunnan, China. Geofluids 16, 56–77.
Spurlin, M.S., Yin, A., Horton, B.K., Zhou, J.Y., Wang, J.H., 2005. Structural evolution of the Yushu-Nangqian region and its relationship to syn-collisional igneous activity, east central Tibet. Geol. Soc. Am. 117, 1293–1317.
Third Geological Team, 1984. The exploration report of the Jinding Zn–Pb deposit in Lanping County, Yunnan Province. Yunnan Bureau Geol. Mineral Resour. 50–106 (in Chinese).
Thode, H.G., Monster, J., Durford, H.B., 1961. Sulphur isotope geochemistry. Geochim. Cosmochim. Acta 25, I50–174.
Torrealday, H., Hitzman, M., Stein, H., Markley, R., Armstrong, R., Broughton, D., 2000. Re–Os and U–Pb dating of the vein-hosted mineralisation at the Kansanshi copper deposit, northern Zambia. Econ. Geol. Bull. Soc. Econ. Geol. 95, 1165–1170.
Vaughan, D., Sweeney, M., Friedrich, G., Diedel, R., Haranczyk, C., 1989. The Kupferschiefer: an overview with an appraisal of the different types of mineralisation. Econ. Geol. 84, 1003–1027.
Wang, G.H., 2010. The Study of Genesis of Jinman-Liancheng Vein Deposits in Lanping Basin, Western Yunnan. Master Degree Thesis. Kunming University of Science and Technology, Kunming, pp. 77 (in Chinese with English abstract).
Wang, Y., Zhu, X.K., 2010. Applications of Cu isotopes on studies of mineral deposits: a status report. J. Jilin Univ. (Earth Science Edition) 40, 739–751 (in Chinese with English abstract).
Wang, Y.J., Zhang, A.M., Fan, W.M., Peng, T.P., Zhang, F.F., Zhang, Y.H., Bi, X.W., 2010. Petrogenesis of late Triassic post-collisional basaltic rocks of the Lancangjiang tectonic zone, southwest China, and tectonic implications for the evolution of the eastern Paleo-Tethys: geochronological and geochemical constraints. Lithos 120, 529–546.
Wang, C.M., Deng, J., Carranza, E.J.M., Lai, X.R., 2014a. Nature, diversity and temporal-spatial distributions of sediment-hosted Pb–Zn deposits in China. Ore Geol. Rev. 56, 327–351.
Wang, C.M., Deng, J., Carranza, E.J.M., Santosh, M., 2014b. Tin metallogenesis associated with granitoids in the southwestern Sanjiang Tethyan Domain: nature, deposit types, and tectonic setting. Gondwana Res. 26, 576–593.
Wang, C.M., Deng, J., Lu, Y.J., Bagas, L., Kemp, A.I.S., McCuaig, T.C., 2015a. Age, nature, and origin of Ordovician Zhibenshan granite from the baoshan terrane in the Sanjiang region and its significance for understanding proto-Tethys evolution. Int. Geol. Rev. 57, 1922–1939.
Wang, C.M., Deng, J., Santosh, M., Lu, Y.J., McCuaig, T.C., Carranza, E.J.M., Wang, Q.F., 2015b. Age and origin of the Bulangshan and Mengsong granitoids and their significance for post-collisional tectonics in the Changning-Menglian Paleo-Tethys Orogen. J. Asian Earth Sci. 113, 656–676.
Wang, C.M., Bagas, L., Lu, Y.J., Santosh, M., Du, B., McCuaig, T.C., 2016a. Terrane boundary and spatio-temporal distribution of ore deposits in the Sanjiang Tethyan Orogen: insights from zircon Hf-isotopic mapping. Earth-Sci. Rev. 156, 39–65.
Wang, Y.H., Zhang, F.F., Liu, J.J., Que, C.Y., 2016b. Carboniferous magmatism and mineralization in the area of the Fuxing Cu deposit, Eastern Tianshan, China: evidence from zircon U-Pb ages, petrogeochemistry, and Sr–Nd–Hf–O isotopic compositions. Gondwana Res. 34, 109–128.
Wang, Y.H., Zhang, F.F., Liu, J.J., Que, C.Y., 2016c. Genesis of the Fuxing porphyry Cu deposit in Eastern Tianshan, China: evidence from fluid inclusions and C-H–O–S–Pb isotope systematics. Ore Geol. Rev. 79, 46–61.
Wang, C.M., Chen, J.Y., Yang, L.F., Zhang, D., Shi, K.X., 2017a. Tectonic-fluid-mineral system in the Lanping basin, Sanjiang Tethys. Acta Petrol. Sin. 33, 1957–1977 (in Chinese with English abstract).
Wang, C.M., Deng, J., Bagas, L., Wang, Q., 2017b. Zircon Hf-isotopic mapping for understanding crustal architecture and metallogenesis in the Eastern Qinling Orogen. Gondwana Res. 50, 293–310.
Warren, J.K., 2000. Evaporites, brines and base metals: low-temperature ore emplacement controlled by evaporate diagenesis. Aust. J. Earth Sci. 47, 179–208.

Weinstein, C., Moynier, F., Wang, K., Paniello, R., Foriel, J., Catalano, J., Pichatb, S., 2011. Isotopic fractionation of Cu in plants. Chem. Geol. 286, 266–271.
Wen, N., Boyce, A.J., Fallick, A.E., Ashworth, J.R., Ixer, R.A., 1996. The genesis of Cu-bearing quartz veins by metamorphic remobilization from stratiform red bed deposits, SW County Cork, Ireland. Mineral. Petrol. 57, 73–89.
Wu, N.P., Jiang, S.Y., Liao, Q.L., Pan, J.Y., Dai, B.Z., 2003. Lead and sulfur isotope geochemistry and the ore sources of the vein-type copper deposits in Lanping-Simao Basin, Yunnan Province. Acta Petrol. Sin. 19, 799–807 (in Chinese with English abstract).
Xiao, R.G., 1989. Reservation of Thermal Brine with Ore-forming Materials and Abrupt Mineralisation. Postdoctoral report. Institute of Geochemistry, Chinese Academy of Sciences, Guiyang, pp. 77 (in Chinese).
Xiao, R.G., Chen, H.Q., Shuai, K.Y., Yang, Z.F., 1994. Mineralisation of Jinman copper deposit in mesozoic sedimentary rocks in Lanping, Yunnan Province. Geoscience 8, 490–496 (in Chinese with English abstract).
Xu, Q., Mo, X., 2000. Regional fluid characters and regimes of “Sanjiang” middle belt during Neo-Tethys. Acta Petrol. Sin. 16, 639–648.
Xu, X.C., Huang, Z., Xie, Q.Q., Yue, S.C., Liu, Y., 2004. Ar–Ar isotopic ages of Jinman and Shuixie copper polymetallic deposits in Yunnan Province, and their geological implications. Geol. J. China Univ. 10, 157–164 (in Chinese with English abstract).
Yan, W., Li, C.Y., 1997. Geochemical characteristics and their hydrothermal sedimentary genesis of a new type of copper deposit. Geochim. 26, 54–63 (in Chinese with English abstract).
Yang, T.N., Ding, Y., Zhang, H.R., Fan, J.W., Liang, M.J., Wang, X.H., 2014. Two-phase subduction and subsequent collision defines the Paleotethyan tectonics of the southeastern Tibetan Plateau: evidence from zircon U–Pb dating, geochemistry, and structural geology of the Sanjiang orogenic belt, southwest China. Geol. Soc. Am. Bull 10.1130/B30921.1.
Yang, L.F., Shi, K.X., Wang, C.M., Wu, B., Du, B., Chen, J.Y., Xia, J.S., Chen, J., 2016. Ore genesis of the Jinman copper deposit in the Lanping Basin, Sanjiang Orogen: constraints by copper and sulfur isotopes. Acta Petrol. Sin. 32, 2392–2406 (in Chinese with English abstract).
Zeng, P.S., Li, W.C., Wang, H.P., Li, H., 2006. The Indosinian Pulang super large porphyry copper deposit in Yunnan, China: petrology and chronology. Acta Petrol. Sin. 22, 990–1000 (in Chinese with English abstract).
Zeng, P.S., Hou, Z.Q., Gao, Y.F., Du, A.D., 2012. The Himalayan Cu–Mo–Au mineralisation in the eastern indo-Asian collision zone: constraints from Re–Os dating of molybdenite. Geol. Rev. 52, 72–84 (in Chinese with English abstract).
Zhang, J., Chen, Y.J., Pirajno, F., Deng, J., Chen, H.Y., Wang, C.M., 2013. Geology, C–H–O–S–Pb isotope systematics and geochronology of the Yindongpo gold deposit, Tongbai Mountains, central China: implication for ore genesis. Ore Geol. Rev. 53, 343–356.
Zhang, J.R., Wen, H.J., Qiu, Y.Z., Zhang, Y.X., Li, C., 2013. Ages of sediment-hosted Himalayan Pb–Zn–Cu–Ag polymetallic deposits in the Lanping basin, China: Re–Os geochronology of molybdenite and Sm–Nd dating of calcite. J. Asian Earth Sci. 73, 284–295.
Zhang, J.R., Wen, H.J., Zhou, Z.C., Du, S.J., 2015. Origin of CO_2-rich ore-forming fluids in the vein-type Cu deposit in western Lanping Basin, Yunnan: evidence from He and Ar isotopes. Geochimica 44, 167–177.
Zhao, H.B., 2006. Study on the Characteristics and Metallogenic Conditions of Copper-Polymetallic Deposits in Middle-Northern Lanping Basin, Western Yunnan. Ph.D. Dissertation. China University of Geosciences (Beijing), Beijing, pp. 230 (in Chinese with English abstract).
Zhou, X.X., Wang, J.S., Yang, D.Z., Liu, J.H., 2013. H-O–S–Cu–Pb isotopic constraints on the origin of the Nage Cu–Pb Deposit, southeast Guizhou Province, SW China. Acta Geol. Sin. 87, 1334–1343 (English Edition).
Zhu, X.K., O'Nions, R.K., Guo, Y., Belshaw, N.S., Rickard, D., 2000. Determination of natural Cu-isotope variation by plasma-source mass spectrometry: implications for use as geochemical tracers. Chem. Geol. 163, 139–149.
Zhu, X.K., Guo, Y., Williams, R.J.P., O'nions, R.K., Matthews, A., Belshaw, N.S., Canters, G.W., de Waal, E.C., Weser, U., Burgess, B.K., Salvato, B., 2002. Mass fractionation processes of transition metal isotopes. Earth Planet. Sci. Lett. 200, 47–62.
Zhu, B., Kidd, W.S.F., Rowley, D.B., Currie, B.S., Shafique, N., 2005. Age of the initiation of the Asia-Central Himalaya. J. Geol. 113, 265–285.